J Appl Electrochem (2014) 44:23–43
DOI 10.1007/s10800-013-0628-0

REVIEW PAPER

In situ Raman spectroscopic–electrochemical studies of lithium-ion battery materials: a historical overview

Victor Stancovski · Simona Badilescu

Received: 13 July 2013 / Accepted: 16 September 2013 / Published online: 2 October 2013

Abstract In this review, the recent advances in the development of in situ Raman spectroscopy and electrochemical techniques and their application for the study of lithium-ion batteries are revisited. It is demonstrated that, during a relatively short period of time (1995–2013), the spectroelectrochemical techniques used for the investigation of battery components, benefited directly from the tremendous advances of Raman technology. The most important step was the implementation of confocal Raman microscopy in the battery research, which opened the way to new and more sophisticated applications. This review shows how the discovery of new Raman techniques such as surface-enhanced Raman scattering, tip-enhanced Raman spectroscopy, spatially offset Raman spectroscopy as well as the integration of Raman spectrometers into non-optical microscopes, for example AFM and SEM, allowed to perform two or more analytical techniques on the same sample region, with an exceptionally high resolution. All these progresses led to new insights into battery materials and components such as electrodes and electrolytes, and helped to understand the electrode/electrolyte interface phenomena. This enhanced understanding allowed a deeper insight into important phenomena, as e.g., battery aging and the dynamic nature of the solid electrolyte interfaces in lithium batteries. The high relevance of the information provided by these techniques in the progress of battery modeling is another positive contribution. Another area of high practical significance for the battery field is the screening of electrode materials, which is facilitated by the availability of the data provided by spectroscopic methods.

Keywords Lithium-ion battery · Raman history · Solid electrolyte interphase · In situ techniques · Confocal Raman microspectrometry

V. Stancovski
LogiCoul Solutions LLC, 1924 Klingensmith Rd., Suite #72, Bloomfield Hills, MI 48302, USA

S. Badilescu (✉)
Mechanical and Industrial Engineering, Concordia University, 1455 Boul. de Maisonneuve O., Montreal, QC H3G 1M8, Canada
e-mail: simonabadilescu0@gmail.com

1 Introduction: historical perspective

The importance of energy storage in all areas of human activity is significant, and growing. Transportation, smart grid, life-sustaining medical devices are only some of the evolving fields in which better batteries play a critical role. Lithium (Li)-based battery chemistries play an increasingly important role in all these areas, primarily owing to their high energy density.

The improvement of batteries is a difficult task, both from the scientific and the technical viewpoints. New electrochemical systems reach the marketplace only once every few years, and the energy density of the Li batteries increased on the average only by 8–9 % a year since the early 1990's [1]. In this context, it is clear that the more detailed the information acquired about the composition of a battery and its changes at nanoscale, the more effective the improvement efforts will become. The investigation of the structure of batteries and its changes is quite difficult, because of the complexity of the interactions between the local chemistry and the electric fields acting during charging, discharging, and at rest.

Raman spectroscopy plays a major role in these investigations. Key advances in Raman techniques were, and are, instrumental in understanding the way batteries work.

Our intention is to emphasize what the Raman techniques corresponding to the different stages of development in Raman technology had added along the way to our knowledge about batteries. For this purpose, we believe that it is appropriate to introduce in the text short explanatory notes on the instruments and techniques used in different laboratories. As our paper will follow the Raman work on batteries in a chronological order, the reader will see the significance of the advances made in Raman instrumentation. Different investigation methods are working in tandem. Information coming from one method may be reinforced or contradicted by studying the phenomenon with another method. We tried to broaden our perspective and compare results, whenever this was possible. A perusal of the publications focused on Li-ion batteries reveals clearly the importance of the continuity in research.

The phenomenon of Raman scattering was discovered in 1928 by C.V. Raman, honored for his discovery with the 1930 Physics Nobel Prize. The results of his first experiments were published in Nature [2]. Later, in the same year, Landsberg and Mandelstam reported the same phenomenon [3]. Together with IR spectroscopy, Raman spectroscopy laid the foundation of vibrational molecular spectroscopy. In spite of the technical difficulties of the beginning, fundamental studies on thousands of compounds were reported. Critical advances in the instrumentation, such as the introduction of photoelectric detectors in the 1940s and the availability of lasers as monochromatic Raman sources (in the 1960s), stimulated the renaissance of Raman spectroscopy. Double-grating as well as holographic monochromators were designed for Raman spectrometers before the 1970s. During the next decade most of the research instruments were using triple spectrographs with multichannel detectors, introduced by Dilor, Jobin-Yvon, and Spex. A major step ahead, paving the way toward the birth of the modern Raman spectroscopy, was the coupling of the Raman spectrometer to an optical microscope, a concept envisaged by Delhaye and Migeon in 1966 [4].

The first prototype of a commercial instrument—the molecular optics laser examiner Raman microscope—was presented in 1974 at both L'Universite des Sciences et Techniques de Lille in France and the National Bureau of Standards in Washington [5–7]. A year before, Delhaye's group reported on the performance of the new instrument at the Fourth international conference on Raman spectroscopy. They have demonstrated that high nominal apertures allow Raman collection from almost 2π steradians, if the optical coupling between the microscope and the spectrometer is right. The lack of sensitivity of this instrument, due to high background levels, will be overcome only later (in the mid 1980s), after the implementation of high-sensitivity low-noise multichannel detectors such as the charge-coupled device (CCD) detectors.

The introduction of confocal microscopy (around 1990) provided improved contrast to Raman maps and a better depth resolution. Because of the relevance of confocal Raman microscopy for battery research, it will be presented separately later; in direct connection with specific publications.

The incorporation of Raman spectrometers into non-optical microscopes, such as SEM and atomic force microscopy (AFM), improved substantially the spatial resolution and made possible the direct connection of Raman spectra to local morphological features.

This configuration leads to the transformation of the Raman spectrum from a measurement of the macroscopic properties into a local indicator of chemical information.

Among the latest additions to integrated systems is near-field Raman spectroscopy, where a scanning near-field microscope is integrated with a Raman spectrometer.

In this review paper, we are following the evolution of information on electrode materials, solid electrolyte interface (SEI), electrolytes, and whole batteries, as determined by the progress in both spectroelectrochemical cells and Raman instrumentation. Looking at the schematic representation that shows the approximate time line of the development of Raman technology (Fig. 1), one can immediately realize that, at the time when this survey begins (1995), Raman spectroscopy was already integrated with microscopy. New developments such as integration with AFM, and techniques such as Fourier transform-Raman and surface-enhanced Raman scattering (SERS) were rapidly joining the Raman arsenal. Tip-enhanced Raman spectroscopy (TERS) combined Raman spectroscopy with a local electromagnetic (EM) near-field enhancement and provided a new approach for studying nanomaterials.

More recently, a new technique called spatially offset Raman spectroscopy (SORS) was discovered and investigated by Matousek and collaborators at the Rutherford Appleton Laboratory in the UK [9]. While conventional Raman spectroscopy is limited to near-surface regions, SORS permits the retrieval of Raman spectra of deeper layers. Inexpensive modular laser Raman spectrometers based on CCD detection were introduced by companies such as Ocean Optics and Boston Advanced Technologies, Inc. [10].

We feel that, as this survey covers almost two decades of research in the field of LIB batteries, it is only too right to cite as frequently as possible the groups and the laboratories where the work was performed. At the same time,

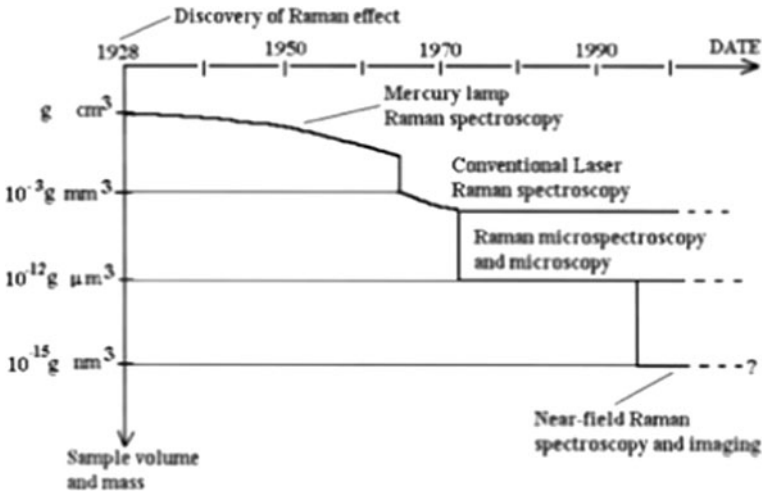

Fig. 1 Evolution of instrumentation for detection of the Raman effect as driven by the available technologies. Reprinted from [8]. Copyright (2007), with permission from the American Chemical Society

we intend to mention the companies involved in bringing about the progress in Raman technology. Taking into account the huge number of publications in the field of batteries, it is understood that this review cannot be comprehensive. The selection of papers is focused largely on the advances in Raman instrumentation and the consequences for the science of batteries. A comprehensive and thorough review, where the interested reader can find Raman data corresponding to a wide range of electrode materials, is that of Baddour-Hadjean and Pereira-Ramos [11]. In spite of the different foci (material-oriented vs instrument-oriented, respectively), an incidental overlap of information was unavoidable.

2 In situ Raman measurements: Li insertion in graphite and other types of carbon

In the context of measurements, "in situ" means that samples are measured in their natural position or place. In the case of Raman studies, this refers to studies inside the electrochemical cell. Under the appropriate experimental conditions, Raman is a nondestructive and noninvasive technique. The importance and advantages of using in situ techniques for spectroscopic and microscopic studies on battery materials was emphasized by Aurbach et al. [12, 13], as well as by Odziemkowski and Irish [14].

The need for using in situ techniques is a consequence of the high reactivity of Li-based and other battery materials not only with the atmospheric components, but also with aprotic solvents such as alkyl carbonates as well. Even in a glove box, in an argon (Ar) atmosphere containing traces of water, oxygen, or carbon dioxide at ppm level, Li is reactive and, for this reason, in situ methods have to be used whenever this is possible. Otherwise, very carefully designed devices have been used to transfer the samples from the inert atmosphere of a glove box to the Raman instrument or any other analytical chamber [15]. For TEM, AFM, and FTIR measurements, samples were often prepared in the glove box and sometimes, in a "flow through" type glove box [16]. The authors called the method "semi-in situ" when measurements were performed in a controlled atmosphere [17]. When using techniques such as X-ray photoelectron spectroscopy (XPS), the high vacuum would remove the volatile components and produce irreversible changes in the materials. For this reason, the advanced in situ methods such as those used today are invaluable tools for the characterization of battery materials and interfacial phenomena.

The first in situ cell, used by Inaba et al., a simple homemade cell is shown in Fig. 2a.

The first cell (Fig. 2a) was made of pyrex glass and the sample was attached to a stainless steel rod, close to the optically flat glass facing the laser beam. Because of the sensitivity of electrode materials (especially Li) to humidity, the cell is always assembled in an Ar-filled glove box. The authors used a Jobin-Yvon, T64000 triple spectrometer with a CCD detector and the 514.5 nm line of the Ar-ion laser as a source. By using the simple two-electrode homemade cell shown in Fig. 2a, Inaba et al. have investigated Li electrochemical intercalation in highly ordered pyrolytic graphite (HOPG) and in natural graphite powder, as well as the corresponding stage structure of graphite intercalation compounds (GICs). The research on the stage structure of GICs relies heavily on previous Raman and infrared work on many kinds of graphite material and the study of the staging phenomenon was carried out especially at MIT [20–22]. It is important to point out that hexagonal graphite belongs to the D_{6h}^4 space group, and has two allowed Raman modes, E_{2g1} and E_{2g2}, at 42 and 1,581 cm^{-1}, respectively, and, in addition, a line around 1,360 cm^{-1}, associated to the disordered material. It has been found that the measurement of the stage index can be

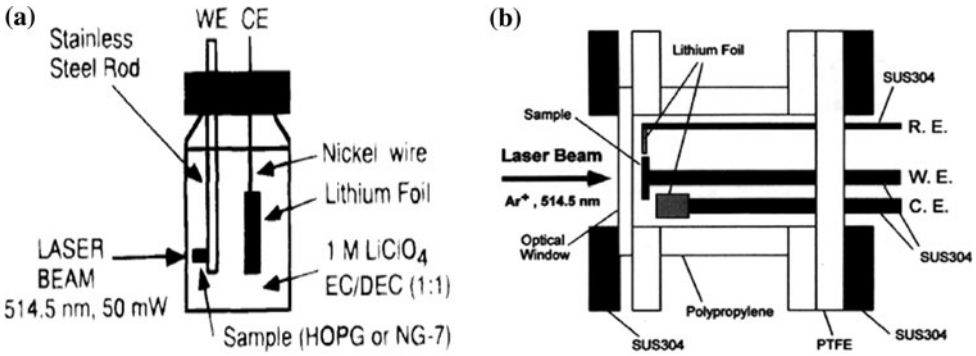

Fig. 2 **a** The first in situ Raman cell used by Inaba's group at Kyoto University [18]. **b** Schematic diagram of the in situ Raman cell used a year later for measurements on MCMBs heat-treated at various temperatures. Reprinted from [19]. Copyright (1996), with permission from The Electrochemical Society

based on the frequency shift of these bands as well as on their relative intensity [23].

The charging curve showed three plateaus associated to reversible phase transitions, which were correlated with the Raman spectral changes. It is important to emphasize the good agreement of the Raman results with Dahn's in situ XRD results [24]. This agreement reinforced the idea of developing Raman spectroscopy as a complementary tool to X-ray diffraction, for the study of GICs. The next year, Inaba's group used a similar but three-electrode cell with Li foil counter and reference electrodes. The electrolyte was a mixture of EC and DEC containing 1 M $LiClO_4$. The new cell shown in Fig. 2b was made of polypropylene and teflon with a pyrex optical window. An Ar-ion laser was used to irradiate the electrode surface through the optical window. Li insertion was carried out between 0 and 2.0 V.

The work is especially interesting because mesocarbon microbeads (MCMBs), classified as a soft carbon, have been proposed, at the time, as a promising anode material in the secondary Li batteries. The interest for this material was due to its very high capacity, 750 mAh/g, compared with that of the graphite of only 372 mAh/g. For this reason, the authors attempted to clarify the mechanism of Li insertion into MCMBs, heat-treated at various temperatures. For the material treated at high temperatures, the E_{2g2} band showed the formation of staged GICs upon Li insertion between graphene layers. They found that, in agreement with XRD results, at high temperatures (above 2,000 °C), MCMBs are graphitized and the Raman bands appear broadened (Fig. 3), indicating an increase in the disorder. They showed that, while at high temperatures Li is inserted between organized graphene layers, in the case of the material heat-treated at lower temperatures (700 °C) the high discharge capacity originates from Li inserted into regions without an organized graphitic structure.

Structures even more disordered than that of MCMB's such as polyparaphenylene (PPP)-based carbon were studied by Endo et al. at MIT [25]. Because of its highly disordered structure, PPP has the high Li storage capacity of 1,100 mAh/g. The cell used for in situ Raman experiments was made of a non-reflective quartz plate (Fig. 5). A

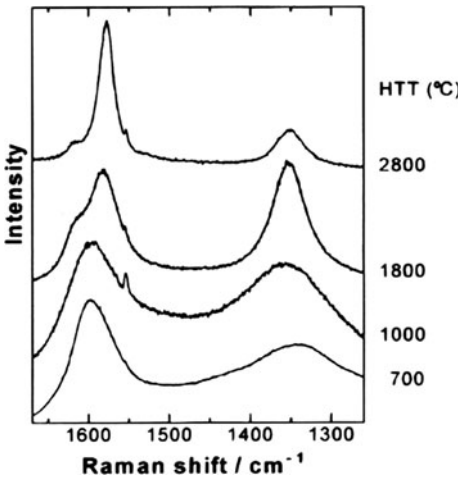

Fig. 3 Raman spectra of MCMBs heat-treated at 2800, 1800, 1000, and 700 °C. The spectra are measured under ambient conditions. Reprinted from [19]. Copyright (1996), with permission from The Electrochemical Society

sample heat-treated at 700 °C was coated on a copper foil attached to a nickel wire and a Li foil attached to the Ni mesh. Charging and discharging in the range 0–2.8 V during the Raman experiment, against the carbon anode (at a current density of 30 mA/cm^2), were monitored by a potentiostat/galvanostat. The excitation source was the 632.8 nm HeNe laser line and the Raman instrument was coupled to a standard Olympus microscope and a collection optical system, the Renishaw Raman Image Microscope System 3000. The laser spot diameter reaching the sample was around 3 μm. This system is a compact laser Raman microscope that can collect both Raman spectra and images through a collection optics, based on a standard Olympus microscope. The samples, placed under the objective (5×, 20×, 50×), are excited by the laser directed through the microscope, and the scattered light is collected by 180° backscattering, next to the optical path corresponding to the incoming laser as shown in Fig. 4. Raman scattered light passes through a notch filter through a grating that disperses the scattered light over a CCD array detector. The spatial resolution of the mapping achieved with this configuration was 1–5 mm (Fig. 5).

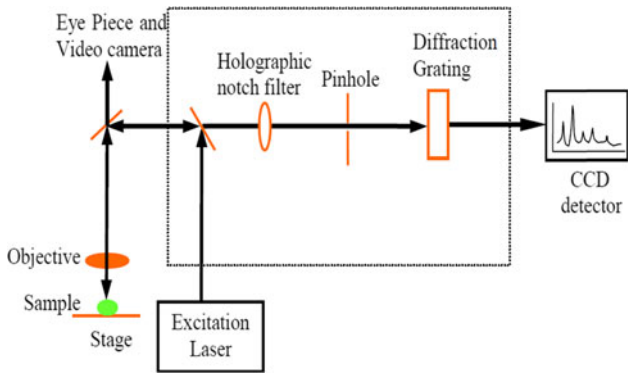

Fig. 4 Schematic diagram of a CCD-based dispersive Raman spectroscopy system where the CCD detector records the Raman spectrum of the sample at the focus point

The source of a Raman spectrometer is, generally, a low-power continuous wave HeNe laser, not exceeding 1 mW radiating power. The laser is enclosed in a protective housing and, according to the laser hazard classification it is a Class 2 laser. However, laser equipment should be labeled, indicating hazard classification, output power, and lasing material [Occupational Safety & Health Administration (OSHA)]. [26].

A Raman spectrum yields information only about the local composition of a sample, while Raman imaging could provide the spatial distribution of structural and chemical information in a heterogeneous sample, as it will be discussed later.

PPP heat-treated at 700 °C is known to have a quinoid-like structure. The results show that during the first discharge and charge cycle, the capacity is much lower than that for a normal cell. In the electrochemical cell used in this work, the carbon materials are positive electrodes, that is, the intercalation of Li takes place during the discharge process. This low capacity is accounted for by the small surface area of the PPP-700 electrode due to the dimensional configuration of the Raman cell, and also by the formation of solid electrolyte interphase (SEI) due to electrolyte decomposition. The voltage dependence of the high-frequency band is shown in Fig. 5b. The authors investigated the structural changes that take place at various voltages in detail, as reflected by the Raman spectra, through the changes in the position and shape, mostly, of the peak around 1,600 cm^{-1}. The position and the shape of this band are associated to the mechanism of Li intercalation. At high voltages (2.8 to $\sim$1.0 V), Li is inserted in the preferred binding sites in PPP-700, without charge transfer, while in the lower voltage range (1–0.04 V), the intercalation is found to be similar to the staging phase transition observed in GICs [27]. The authors concluded that the relationship between the structure and the electrochemical properties has to be established separately for each type of carbon because of the specific morphologies.

3 Introduction to confocal Raman microscopy

The first Raman study of a Li/polymer electrolyte symmetric cell by using confocal Raman micro spectrometry was published in 1998 by Rey et al. [28, 29] at the Laboratoire de Physico-Chimie Moleculaire, Universite de Bordeaux.

The schematic view of the Raman spectroelectrochemical cell used by Rey et al. is shown in Fig. 6.

3.1 Confocal Raman microscopy: introduction

The concept of confocal microscopy was developed by Minsky at Harvard University in the mid-1950s, but the utility of confocal imaging was demonstrated only much later, due to advances in laser and computer technology [30].

The application of confocal microscopy to Raman imaging was first suggested by Delhaye et al. [31]. Compared to the

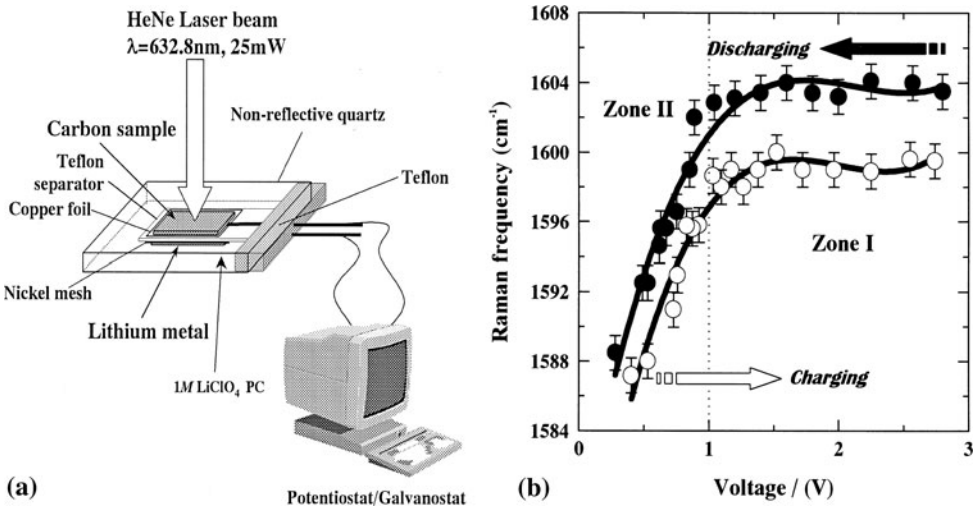

Fig. 5 **a** Schematic representation of the in situ Raman experiment. **b** The voltage dependence of the high-frequency Raman band. Reprinted from [25]. Copyright (1998)

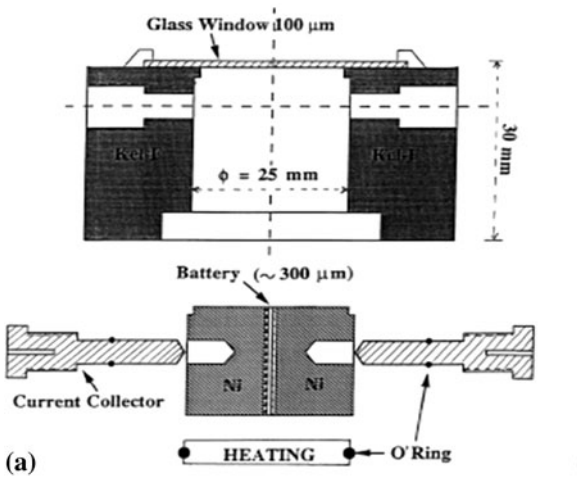

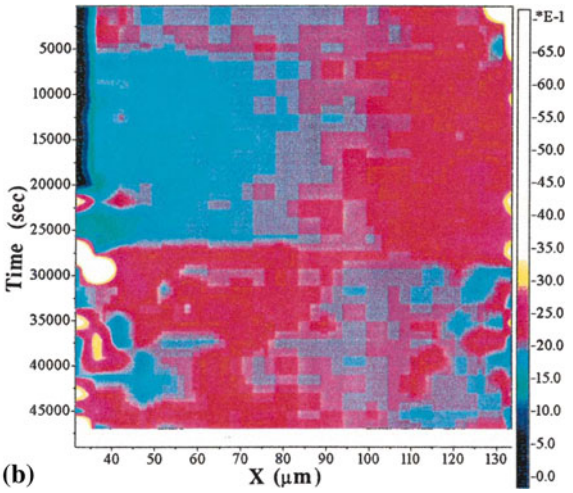

Fig. 6 **a** Schematic view of the main elements of the Raman spectroelectrochemical cell in the electrolyte for the symmetrical cell Li/P(EO)$_{20}$–LiTFSI/Li. The current density is zero for $t < 5000$ s, +0.4 mA/cm^2 for $5000 < t < 27000$ s, and −0.4 mA/cm^2 for $t > 27000$ s. The right scale associates a color to the intensity at each point. Spurious points at the left and right part of the image are situated on defects of the Li electrodes. The data are recorded at 85 °C with the ×50 objective and a 500 μm pinhole. Raman imaging with the Labram 1B spectrometer is done by coupling the spectrometer to a confocal microscope (300 μm pinhole) and an XY-motorized table (0.1 μm steps). The electrochemical cell is adjusted below the microscope objective on a motorized 2D actuator system. Reprinted from [29]. Copyright (1998), with permission from The Electrochemical Society

traditional wide-field optical microscope, the confocal microscope has an enhanced resolution and, most importantly, the capability to collect optical sections from thick samples.

Figure 7 shows that in the configuration of a confocal microscope there are two pinhole apertures—one, right after the source that will reduce the stray light, and a second one, in the front of the detector. In this way, the small pinhole aperture, refocused through the microscope objective, will illuminate only one point on the sample.

Figure 8 shows that in traditional wide-field illumination, a wide cone of illumination is focused over a large volume of the sample, while in point-scanning confocal microscopy the size of the confocal spot ranges between 0.25 and 0.8 μm. The 3D surface of a sample can be reconstructed from the *X*–*Y*–*Z* scan (Fig. 9a). A surface profile can be obtained by using an auto-focusing technique as shown in Fig. 9b. Confocal spectroscopy allows to collect a signal from a single point on a sample as shown in Fig. 10.

When a confocal microscope is combined with a spectrometer, a spectrum can be obtained from a single point on a sample. In the case of confocal Raman microscopy instrumentation, the Raman shift obtained from different spots of the sample will give information on the presence of different species in the sample and their concentration.

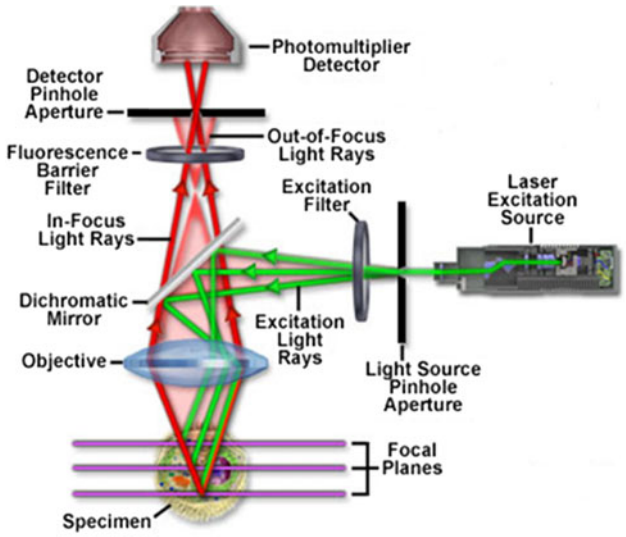

Fig. 7 Optical configuration of a laser scanning confocal microscope. Reprinted from [32]

Fig. 8 Wide field versus confocal point scanning of specimens. Reprinted from [33]

3.2 Characterization of a Li battery by confocal Raman microspectrometry: Raman imaging

The Raman cell shown in Fig. 6 allowed the examination of a battery composed of a thick Li foil (120 μm), a polymer electrolyte (70–100 μm) (PEO)$_{20}$, LiN(SO$_2$CF$_3$)$_2$, and a cathode based on V_2O_5 [28]. The "optical sectioning" of the sample is realized with a pinhole of variable

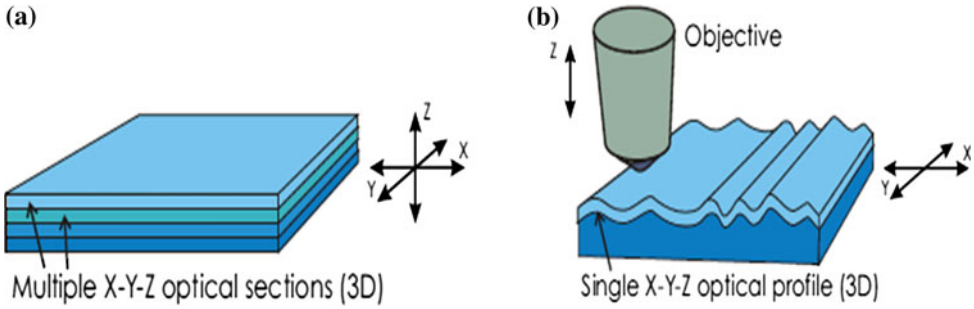

Fig. 9 3D mapping: multiple *X–Y–Z* optical sections (**a**) and a single *X–Y–Z* profile (**b**) obtained in auto-focus mode

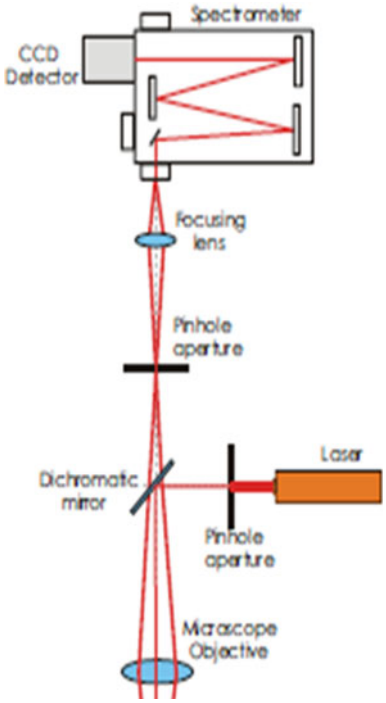

Fig. 10 Optical scheme for confocal spectroscopy including a confocal microscope, spectrometer, and multi-channel CCD detector

aperture, placed at the image plan of the microscope. Spectra are measured along a line of points between the two electrodes. In this way, plenty of information can be obtained, not only on the electrolyte but also on the Li interface and the V_2O_5 cathode. Raman imaging is a powerful technique for generating detailed chemical images based on the Raman spectrum of a sample. A complete spectrum is acquired at each and every pixel of the image, and then interrogated to generate false color images based on the material's composition and structure. Raman imaging is widely used to characterize the distribution of components within a sample, but in addition it is sensitive to material concentration, phase, stress/strain, and crystallinity.

The authors studied a symmetrical [Li/$(PEO)_{20}$-LiTFSI/Li] battery to calculate the concentration gradient in the electrolyte. They used the 742 cm^{-1} ($\delta_s CF_3$) line of TFSI to monitor the concentration of salt in the electrolyte. The two-dimensional plot of the intensity in function of time is shown in Fig. 6b. It can be seen that for times between 5000 and 27000 s, the polarization (0.4 mA/cm^2) induced an increase of the salt concentration toward the anode and when the current is reversed, the concentration gradient is reversed as well.

This is a new and interesting technique for in situ studies of a Li battery, specifically, for measuring the salt concentration gradients in the electrolyte. The polymer electrolyte is placed between the two Li electrodes and heated in situ. Observations are made at a depth of about 20 μm within the electrolyte. The local salt concentration is measured as a function of time, current density I, and electrolyte thickness, and salt diffusion coefficient and ionic transport numbers can be determined.

Two Raman lines have been selected to measure the concentration of the salt at a given point: the narrow band of the anion at 739 cm^{-1} [$\delta(CF_3)$ and $\delta(CH_2)$] of PEO, used as internal reference. A calibration line (the ratio of absorbencies of the two bands) versus $1/n$ = TFSI/EO = Li/EO is shown in Fig. 11.

The methodology and the results obtained in Rey's work represent a big step ahead. The study of the electrolyte would not have been possible without the new capabilities brought about by the confocal micro Raman. They are the first quantitative data on the electrolyte concentration gradient. Actually, preliminary results were obtained by Rey in 1997 [34] but precise measurements on symmetric cells were precluded by technical limitations. However, the concentration profiles obtained in this work were in good agreement with those calculated and reported earlier by Doyle et al. [35] and with Brissot's theoretical predictions [36]. The two groups (Rey's and Brissot's) worked independently on the same topic and their results complemented each other.

Optical concentration measurements were carried out through both in situ and *ex situ* experiments by Brissot et al. [37] at the Laboratoire de Physique de la Matière Condensée (Ecole Polytechnique-CNRS, Palaiseau) on symmetric Li/polymer–electrolyte/Li cells similar to those used by Rey et al. The Li salt used in most experiments was $LiN(CF_3\ SO_2)_2$. Salt concentration maps in the cell were

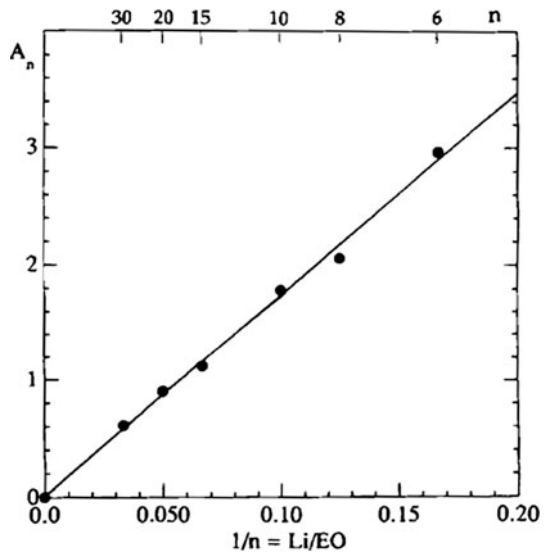

Fig. 11 Variation of $A_n = A[\delta_s\ (CF_3)/A[\delta(CH_2)]$ for $P(EO)_n$–LiTFSI complexes at 80 °C with $30 < n < 6$, as a function of the salt concentration $1/n$. Salt concentration gradients were determined for the Li/V_2O_5 battery as well and a strong increase of the salt concentration toward the anode is observed in discharge. Reprinted from [29]. Copyright (1998), with permission from The Electrochemical Society

obtained during cycling and used for monitoring the evolution of dendrites. The experimental cell is shown schematically in Fig. 12. Li/polymer–electrolyte/Li cells were assembled in a dry box and the nickel collectors were connected to an electrochemical set-up. The cell was introduced in a furnace and heated at 80 °C. The growth of dendrites was studied by studying the concentration inhomogeneities within the electrolyte.

The results of Brissot's optical absorption measurements strongly supported Rey's data obtained by Raman confocal microspectroscopy and contributed to its extension to the study of electrode materials. As a result, Novák et al. [38], working at the Laboratory for Electrochemistry of the Paul Scherrer Institute, used an electrochemical cell developed by the group in conjunction with confocal Raman

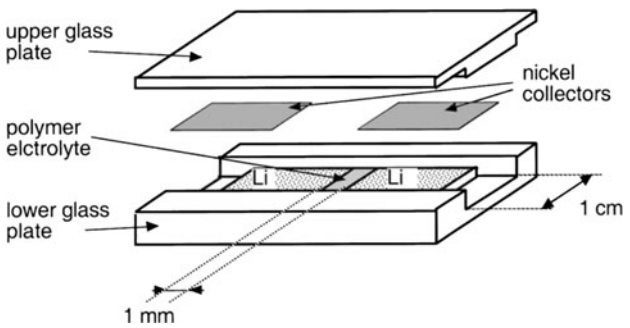

Fig. 12 A schematic view of the electrochemical cell. Reprinted from [37]. Copyright (2001), with permission from Elsevier

spectrometry to study a commercial $LiCoO_2$ electrode. They demonstrated for the first time that the Raman technique is suitable for the characterization of not only carbonaceous materials, but also single oxide particles in positive electrodes of Li-ion cell.

The micro-Raman spectrometer was a DILOR Labram instrument equipped with an Olympus microscope with an internal He–Ne laser and an external Ar-ion laser. Depth up to 0.3 mm can be measured when using an ultralong working distance objective (50×). Low laser power (3–4 mW) was used, to avoid damage to the electrode surface [38, 39]. The Raman spectra of $LiCoO_2$ particles were measured during charging. By adjusting the pinhole diameter to 200 μm, the lateral resolution was 4 μm. The spectra of two particles randomly selected on the surface of a commercial electrode confirmed that the light-colored particles in the photograph shown in Fig. 13b are indeed $LiCoO_2$. During the first galvanostatic charging, the band corresponding to the A_{1g} mode is diminishing with the increasing potential.

The Raman technique was suggested as a fingerprinting technique to evaluate the quality of battery materials after repeated cycling. The authors emphasized the importance of in situ studies (Raman and others) on practical, commercial electrodes and expressed their belief that only in this way, the mechanical and chemical changes in the electrodes and the reactions of the electrolyte at the electrolyte/electrode interfaces can be better understood.

One of the methods that joined the Raman arsenal in the 1970s and allowed the study of these interfaces with a highly improved sensitivity was SERS.

3.3 SERS technique for the study of SEI films

3.3.1 SEI: mechanism of formation

It is generally assumed that, during the first cycle of a graphite electrode, a protective film is formed on the carbon surface due to the reductive decomposition of the electrolyte [15, 16, 40–44]. A schematic illustration of the film-forming mechanism is shown by Besenhard et al. [45] and the intercalation compound is shown in Fig. 14.

Many surface-sensitive tools have been employed for the study of the formation of the SEI. Some surface chemistry aspects of Li-ion batteries are discussed in the review by Aurbach et al. [47]. Interesting results have been obtained with both in situ Raman spectroscopy and in situ video microscopy, by using a confocal Raman microscope equipped with a video camera (Fig. 15).

In situ mass spectroscopy results showed that the evolution of ethylene gas in EC-based electrolytes starts at potentials ~0.8 V versus Li/Li^+ indicating the formation of the SEI.

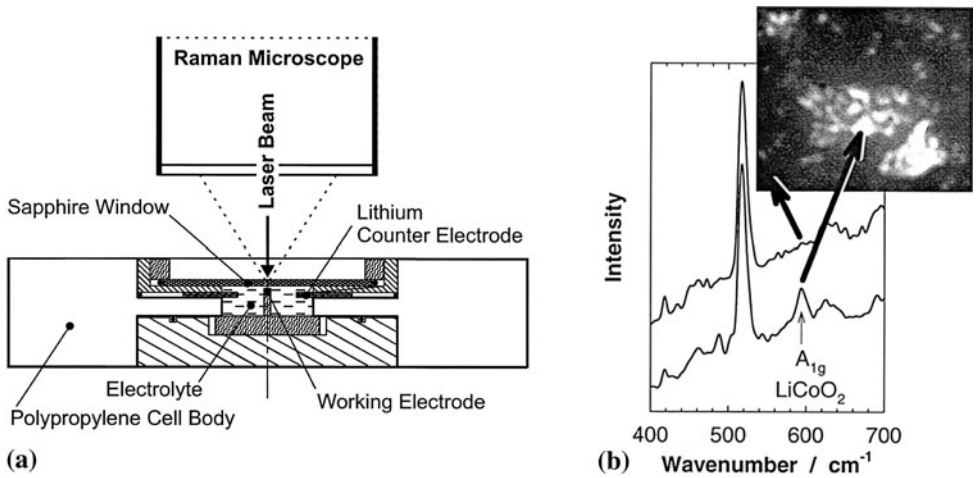

Fig. 13 **a** The electrochemical cell for in situ Raman microscopy. **b** In situ Raman spectra measured on open circuit at the surface of a commercial $LiCoO_2$ electrode in the electrolyte 1 M $LiClO_4$ in EC/DMC (1:1). In the photograph obtained with an optical microscope, which covers an area of approximately 15 × 15 μm, the *arrows* indicate the points where the two spectra were measured. Reprinted from [38]. Copyright (2000), with permission from Elsevier

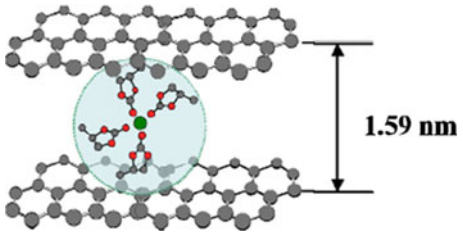

Fig. 14 Schematic illustration of a ternary GIC involving a. solvated Li^+ accommodated between grapheme layers. Reprinted from [46]. Copyright (2010), with permission from Dr. Xu

The discovery of SERS and the application of this new technique to the battery science contributed substantially to the elucidation of electrode/electrolyte interface phenomena.

3.3.2 Introduction to SERS

SERS is a relatively new Raman technique that allows a strong enhancement of the inherently weak Raman signals from Raman-active molecules adsorbed onto specially prepared metal surfaces. It was discovered on a silver electrode by the Fleischmann group in 1974 [48]. This technique makes Raman spectroscopy a sensitive method for surface studies because of the surface enhancement mechanism. The enhancement of the Raman signal can be as high as 10^{14}–10^{16} and the detection sensitivity of SERS has now reached the single-molecule level, under specific conditions [49]. Two enhancement mechanisms have been envisaged in the past [50–52]. The most important enhancement mechanism described in the literature is the EM one, involving the roughness features on a metal surface (Au and Ag) such as nanostructures, gratings, etc.; this enhancement is non-selective chemically. The intensity of the Raman signal is proportional to the magnitude of the EM field created by the nanoparticles and aggregates. In addition to the EM mechanism, a mechanism called chemical enhancement has been suggested. This mechanism is based on the interactions (charge transfer and others) between the molecules and the metal surface, and has been observed for infrared spectroscopy as well [53]. In spite of the less important contribution to the general enhancement (no more than one or two orders of magnitude), this mechanism is interesting, especially when interfacial systems, including electrochemical, catalytic, and biological systems are studied.

TERS is a quite recent technique that uses a metalized scanning probe microscopy tip to scan across a sample. The TERS enhancement is due to the local amplification of the EM field around the tip and the spatial resolution of TERS is of the same order as the radius of curvature of the tip.

3.3.3 Interface phenomena in LIB studied by SERS

SERS was first used on a model system, a rough silver surface in an electrochemical environment, by Irish et al. [54] at the University of Waterloo. The preliminary results obtained in this work were useful later when more sophisticated measurement systems were developed.

A pioneering SERS work, a study of the SEI film in Li-ion batteries, was done by Huang et al. and it was carried out at the Institute of Physics of the Chinese Academy of Sciences in Beijing. In their first work [54], these authors have observed for the first time the surface-enhanced resonance Raman spectrum of rhodamine 6G (a probe molecule) and the surface-enhanced Raman spectrum of the SEI on the surface of Li–Ag alloy formed during the discharge process. SERS has proved to be a suitable technique for the study of SEI as its thickness is normally only about 2 ± 4 nm and the bands are too weak to be observed by Raman spectroscopy.

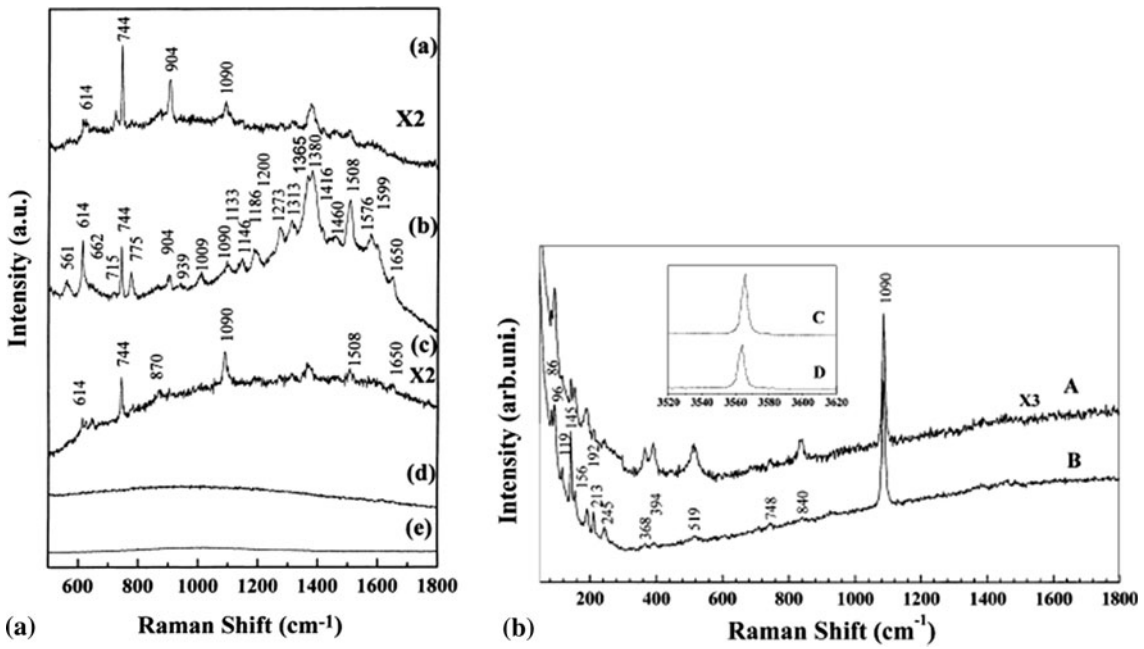

Fig. 15 **a** *Left* SERS spectra of Rh 6G and of the SEI film on Li–Ag alloy electrodes at different discharged states: (*a*) 0.8 V, (*b*) 0.4 V, and (*c*) 0 V, which represents different Li-insertion levels, corresponding to $Li_{<0.01}Ag$, $Li_{<0.1}$ Ag, and Li–Ag, respectively [the intensity of the spectra in (*a*) and (*c*) has been doubled for comparison with (*b*), (*d*), and (*e*)]. (d) The Raman spectrum of Rh 6G adsorbed on Al surface. (*e*) The Raman spectrum of the SEI film on Al sheet after discharging to 0 V; Li–Al alloy was formed at this voltage. Reprinted from [55]. Copyright (2000), with permission from Elsevier. **b** *right* The SERS spectrum of the SEI film on the Ag electrode after discharging to 0 V in a Li/Ag cell. (*A*): Excitation wavelength 514.5 nm Ar^+ line (*B*) 488 nm Ar^+ line. Reprinted from [56]. Copyright (2002), with permission from Elsevier

The authors show that the enhancement effects indicated by the spectra are due to the modification of the morphology of the original Ag electrode sheet through alloying. To complete the work and gather more information on the identity and the structure of species in the SEI film, the same group [56] has studied the SEI film on a discharged to 0.0 V Ag electrode by using a micro-Raman spectrometer (Jobin-Yvon U-1000). The enhancement seen in the spectra is accounted for by the formation of nanostructured Li–Ag alloys. The electrolyte was 1 M $LiPF_6$ in EC and DEC (1:1). The SERS spectrum of SEI film on Ag electrode after discharging to 0 V in a Li/Ag cell is shown in Fig. 17 (right).

The authors concluded that the the Raman signal of the SEI can be surface-enhanced by the Li–Ag alloy and that the reduced species of the solvents and the solute are the main components of the SEI film: Li_2CO_3, $ROCO_2Li$, Li_xPO_y, and $LiOH{\cdot}H_2O$ [18].

3.3.4 Limitations of confocal Raman microscopy for the study of SEI

Further Raman studies carried out by using confocal Raman microscopy as a probing technique [57] clearly evidenced the limitations of confocal Raman microscopy for the study of SEI. In this work, carried out at the Laboratoire de Physico-Chimie Moléculaire, Université Bordeaux, the confocal Raman micro-spectroscopy is used for the investigation of the composition of the passivation layer formed on the surface of commercial Li foils. The authors explained the presence of Li acetylides (Li_2C_2) (1,845 cm^{-1}) by the effect of local heating generated by the laser radiation on carbonate species. The native passivating film consists of an outer layer (1–20 nm) of Li_2CO_3/LiOH on a thicker layer of Li_2O (10–100 nm) which is in direct contact with the Li foil. A Labram 1B spectrometer (Dilor, Jobin-Yvon) with a He/Ne (632.8 nm) laser and a 50× Olympus objective was used. For the in-depth analysis at the polymer electrolyte/Li interface, when using a pinhole of 250 μm at $\lambda_0 = 514.5$ nm, the axial resolution at this interface is around 5 μm for a polymer electrolyte of 50 μm thickness ($n = 1.5$). For surface analysis on Li foils, the pinhole was set at 1,000 μm in order to increase the Raman light output. The cell used for the Raman measurements is shown in Fig. 16a.

Variable intensities are observed for the features around 500 cm^{-1} because the thickness of the passivation layer is not homogeneous. The band at 1,855 cm^{-1} is assigned by the authors to the υ_{C-C} of the triple bond in Li_2C_2. The spectra do not change when Li is exposed to N_2, O_2, CO_2, or CO atmospheres. No line is assigned to Li carbonate (it

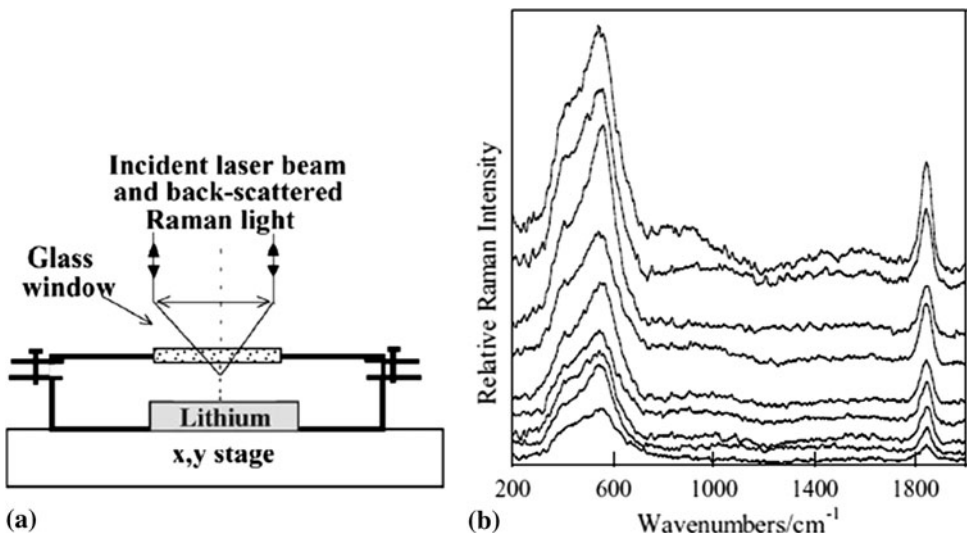

Fig. 16 **a** Schematic drawing of the cell used for the confocal Raman microspectrometry experiments. The cell is installed on a *x*, *y* computer-controlled stage below the microscope. It can also be moved vertically along *z* by steps of 1 μm [56]. **b** Raman spectra of the Li foil recorded at nine different points with an incident wavelength of 632.8 nm, a ×50, NA = 0.55 objective and *P* ca. 1 mW/μm^2. Reprinted from [57]. Copyright (2003), with permission from Elsevier

was found by IR); it is assumed that it is transformed in Li_2C_2s by local heating.

The results of this work show, without any doubt, that Raman spectroscopy is not sensitive enough for the study of SEI, in the absence of an enhancement mechanism. Raman bands can only be seen after the sample is locally degraded under the laser beam.

4 Raman spectromicrotopography of an operating Li-ion battery

Time- and space-resolved measurements of electrodes in an operating battery during discharge have been performed by Scherson's group at Case Western Reserve University [58].

The battery used in this work was a thin Li-ion battery with a carbon anode, a $LiCoO_2$ cathode, and a separator as shown in Fig. 17a. Figure 17c shows the image of the edge obtained by cutting the battery. Both space- and time-resolved in situ spectra were taken in an area close to the center of the battery while charging and discharging the battery at a constant current of 0.2 mA. Spectra were collected with a Chromex Raman 2000 system equipped with an Olympus microscope (20× magnification). The Raman microscope was coupled to a computer-controlled, variable speed, two-dimensional linear translator. The battery was moved under the focused laser beam and during this time, spectra were collected continuously. For the time-resolved spectra, Raman spectra were taken at the same spot on the anode during the discharge process as a function of time (Fig. 18).

The results of this work are particularly valuable for the generation of dynamic images of Li ion transport within the whole battery, images that will be helpful for the assessment of models simulating the flow of Li^+.

5 Mapping of the graphite surface with a high volume resolution (1 μm^3)

Raman single point and mapping measurements of graphite surface by using an improved electrochemical cell were carried out in the Paul Scherrer Institute, by Novak et al. [59].

Figure 19 shows the Raman mapping of the graphite surface, together with the spatial distribution plot of the L_a values. This is the first work to show the correlation of L_a with the morphological features of the surface of the graphite electrode.

5.1 Intercalation of supercapacitor-type electrolyte into microcrystalline graphite and electrochemical doping of single-walled carbon nanotubes (SWCNTs)

Raman microscopy was employed for the study of intercalation of tetraethylammonium and tetrafluoroborate into microcrystalline graphite [59]. The in situ Raman cell used for the collection of the spectra is shown in Fig. 20. The graphite electrode is covered by an aluminum foil and the laser shines on it.

The working electrode of the cell in Fig. 20 is graphite, while the counter and reference electrodes are made of PTFE-bound activated carbon material. After the cell was assembled in air, it was transferred to a glove box where the electrolyte solution was introduced. The laser beam is focused onto the electrode surface with an Olympus objective (80×). The authors found that as an effect of both

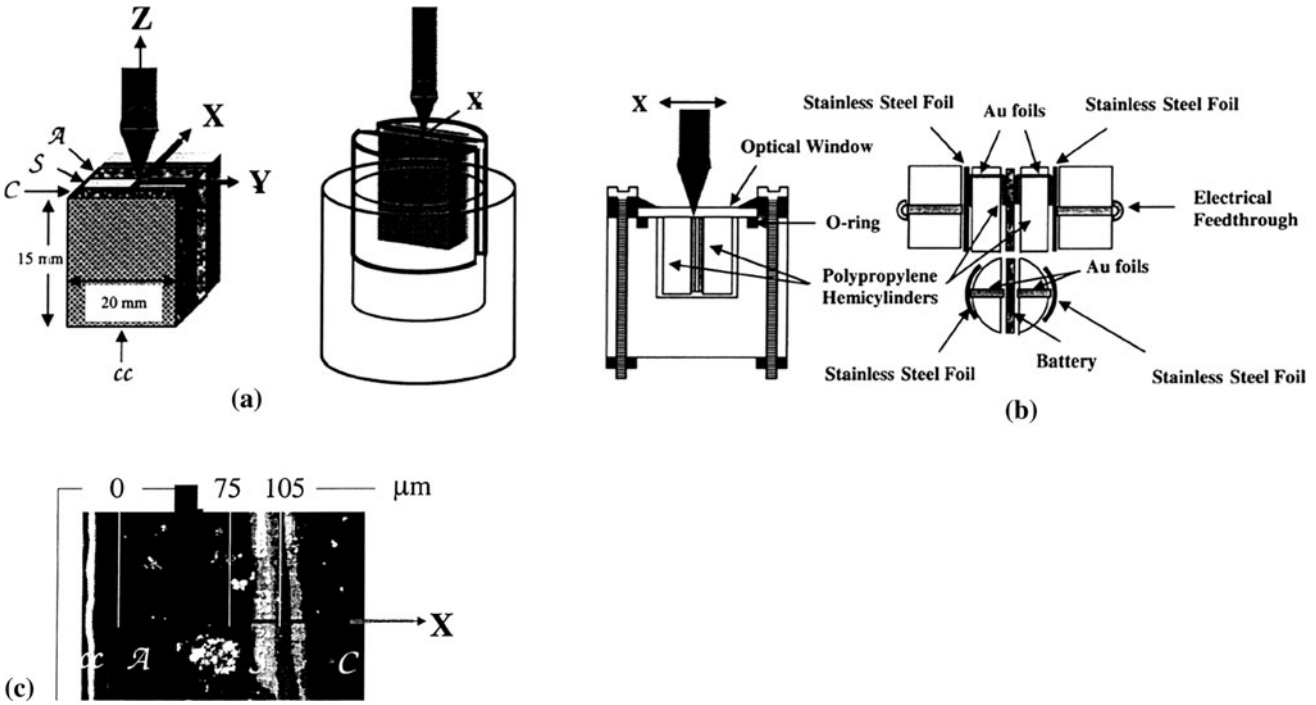

Fig. 17 Schematic diagrams of the battery (**a**), spectroelectrochemical cell (**b**), and microscopic image of a sharp edge of the battery showing the carbon anode (**a** 120–140 μm thick), the separator (*S*, 32–34 μm), the $LiCoO_2$ cathode (*C*, >300 μm thick), and the current collector meshes (cc), i.e., copper (for **a**) and aluminum (for *C*, not shown) (**c**). Raman spectra were collected along the *x*-axis in the direction indicated. Reprinted from [58]. Copyright (2004). Reproduced with the permission of ECS—The Electrochemical Society

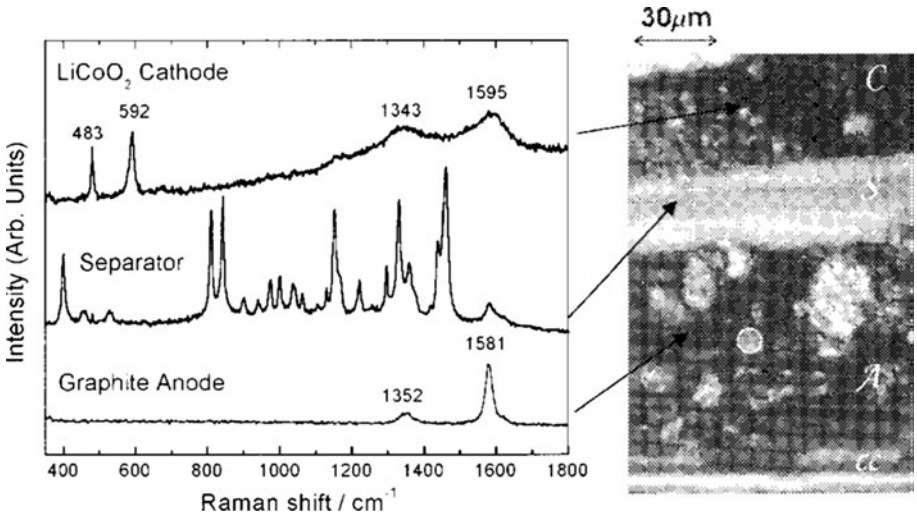

Fig. 18 (*Right*) Image obtained with the microscope attachment of the Raman 2000 showing the layered structure of the Li-ion battery. (*Left*) Raman spectra of random regions of the cathode, *C*; separator, *S*; and anode, *A*. Laser excitation wavelength: 532 nm. The *gray circle* in the picture represents the laser beam image on the battery. Reprinted from [58]. Copyright (2004). Reproduced with the permission of ECS—The Electrochemical Society

insertion and extraction of the two ions (Et_4N^+ and BF_4^-), the G-band of graphite developed into a doublet due to the staged graphite. The results were preliminary but the work demonstrated that the Raman technique can be applied successfully to the study of graphite or other carbonaceous materials in the case of electrochemical double-layer capacitors. The same group at the Paul Scherrer Institute [60, 61] has investigated the electrochemical doping of SWCNTs in a non-aqueous electrolyte (1 M Et_4NBF_4 in acetonitrile), which is relevant for electrochemical double-layer capacitors. The in situ cell was the same as that used in the previous work (shown in Fig. 27) but the working electrode was the SWCNT powder. The authors found that the SWCNT bundles are infiltrated by the electrolyte, resulting in gravimetric integrated capacitances that equal those of activated carbons. From a detailed study, they

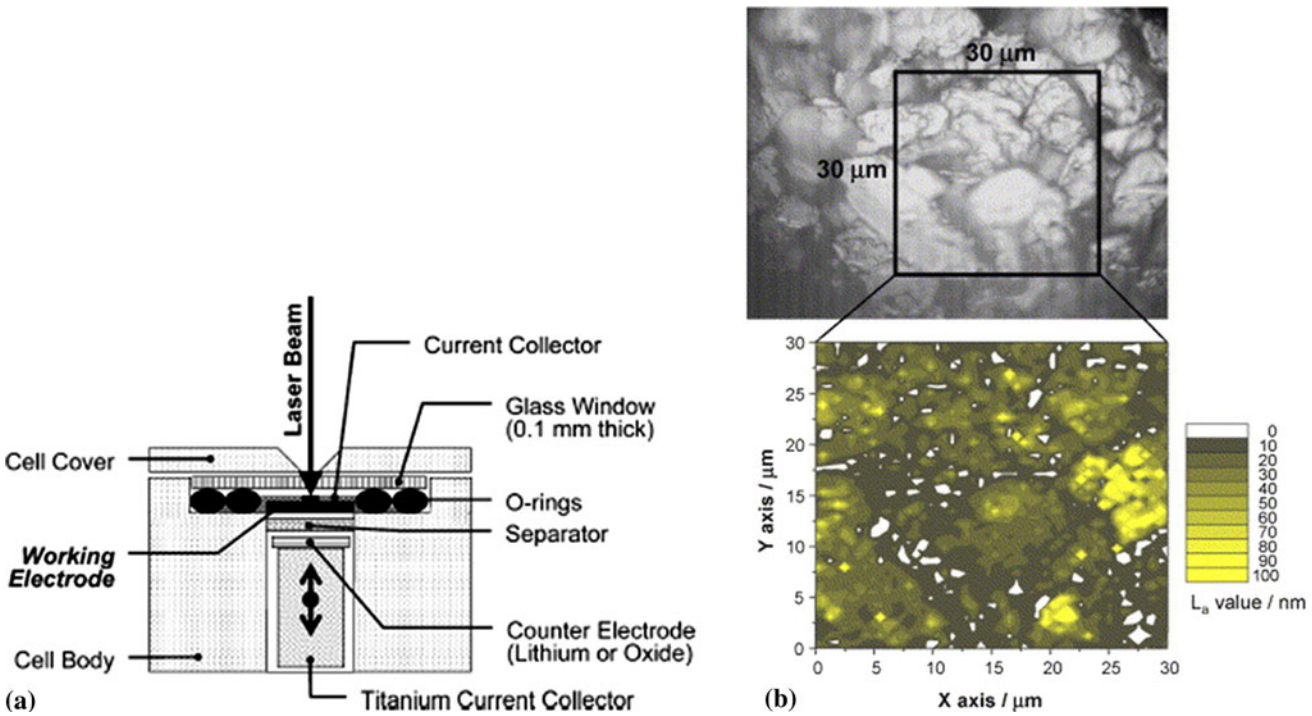

Fig. 19 **a** The electrochemical cell for in situ Raman microscopy. **b** Mapping of graphite surface: Image of a graphite sample (*top*) and spatial distribution plot of L_a values (*bottom*, map 50 × 50 points). L_a is the length of the graphene crystallite sheets. The high volume resolution permitted the study of the surface heterogeneity of the graphite electrode. The advantage of the new configuration of the cell is the proximity of the graphite electrode to the optical window, eliminating the overlap of the Raman spectrum of the electrolyte. Reprinted from [59]. Copyright (2005), with permission from Elsevier

concluded that, at low polarizations, only metallic SWCNTs can be used for charge storage.

The intercalation of a ionic liquid such as 1-methyl-1-propylpiperidinium [bis(trifluoromethylsulfonyl)]imide (MPP_pTFSI) into composite graphite electrodes was studied with cyclic voltammetry by Markevich et al. [62].

The authors used the electrochemical cell shown in Fig. 21. The ionic liquid (or molten salt) studied in this work was a solution based on MPP_pTFSI. Pure IL and IL solutions containing a $LiN(SO_2CF_3)_2$ (LiTFSI) salt were studied. The authors have studied the behavior of graphite electrodes in MPP_p TFSI containing 1 M LiTFSI, in order to understand the phenomena of cointercalation of the IL cation and Li ion as well as the passivation of the graphite surface. An in situ Raman microprobe technique with microscopic lateral resolution, in conjunction with cyclic voltammetry is used for real-time monitoring and the Raman spectra were collected from five selected points. The electrochemical responses were measured simultaneously. The intercalation of IL cations into the graphite structure was evidenced by the development of the 1,602 cm^{-1} shoulder of the G-band during the charging at a potential higher than 0.3 V versus Li/Li^+. The process of Li-ion intercalation with the formation of Li–GICs was demonstrated by the emergence of the E_{2g2} (b) band at 1,602 cm^{-1} at potentials about 0.2 and 0.3 V versus Li/Li^+. Because of the heterogeneity of the electrode material and the different local surface conditions, differences in the behavior of the different points on the electrode were observed. The Raman spectra indicated the coexistence of the two intercalation processes during the first three cycles and the passivation of the graphite electrode by surface film formation.

6 Next-generation electrode materials

Advances in solid-state chemistry led to the development of various candidate cathode materials with high cyclic stability and a high reversible specific charge. Because of their low cost, abundance, and non-toxicity, transition-metal-layered oxides with excess Li are emerging as the most promising high energy density cathode materials for the next-generation electrode materials. They are considered to be solid solutions of the type $(x)\ Li_2MnO_3(1-x)\ LiMO_2$ (M = Mn, Ni, or Co) and are also known as "layered–layered" composite cathode systems. The challenges and prospects of the high-energy layered cathode materials are discussed in a recent review paper [63].

Li_2MnO_3 is known to be electrochemically inactive because Mn is in its +4 oxidation state. However, it has

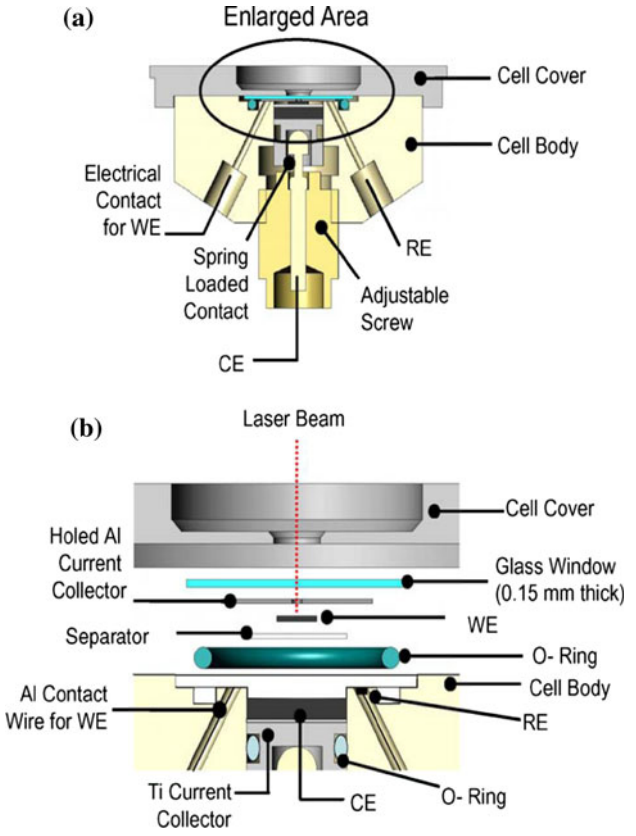

Fig. 20 Three-electrode in situ Raman cell in (**a**) the fully assembled stage and (**b**) an enlarged area showing the separate components (expanded, not to scale). This is a upgraded Raman cell that allows measurements with a reference electrode (previously: two-electrode set-up). The electrochemical intercalation of tetraethylammonium (Et_4N^+) and tetrafluoroborate (BF_4^-) into and out of microcrystalline graphite is studied. Reprinted from [60]. Copyright (2006), with permission from Elsevier

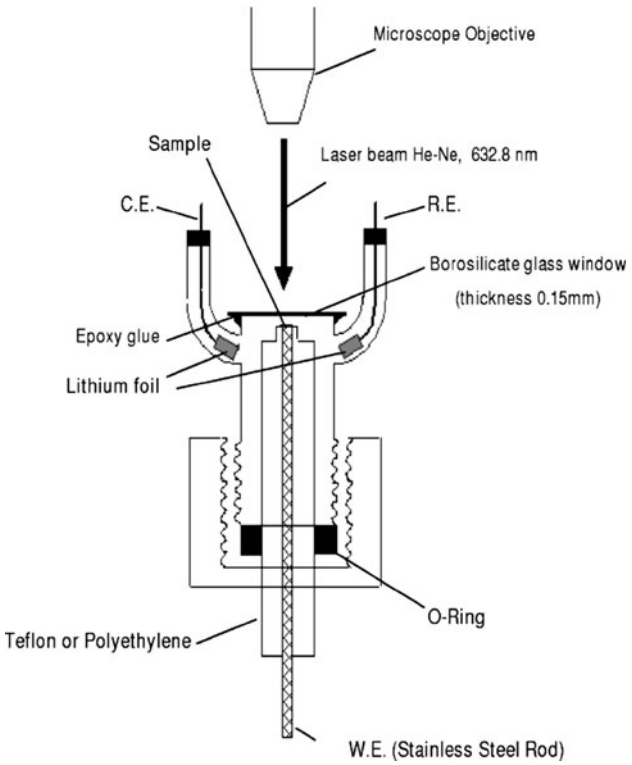

Fig. 21 Schematic view of the electrochemical cell used for in situ Raman measurements: three-electrode spectroelectrochemical cell (pyrex, air-tight). Micro-Raman spectrometer HR 800 (Jobin-Yvon Horiba), power limited to <0.3 mW to avoid local heating of graphite, spectra collected from five arbitrarily selected points, ambient temperature. The cell was assembled in a glove box, under Ar gas. Reprinted from [62]. Copyright (2008), by permission of The Electrochemical Society

been shown that when charging the cathode above 4.5 V, the material is activated electrochemically due to the simultaneous extraction of Li and O, and the activation results in the formation of the MnO_2 host structure which can reversibly intercalate Li ions.

Both *ex situ* [64] and in situ Raman spectroscopy at elevated temperatures [65] were instrumental in elucidating the activation mechanism of Li_2MnO_3. It has been demonstrated that, during the initial charging, the layered structure of Li_2MnO_3 is transformed into a spinel-like phase. At 60 °C, after the first charge at 4.7 V, the Raman spectrum showed a pronounced blue shift of the peak, accompanied by a decrease of the intensity. The authors accounted for the changes by a Li de-intercalation from the structure and the formation of a cubic Li–Mn spinel phase.

Similarly, under in situ conditions, at 50 °C, upon charging, it was found that the A_g band was shifted toward higher wavenumbers (from 615 to 630 cm^{-1}). The authors have assigned the observed shift to the partial formation of a spinel-like phase.

A Raman study of a similar layered compound ($Li_{1.2}Ni_{0.175}Co_{0.1}Mn_{0.52}O_2$) has shown that, in the range of 4.1-4.4 V, the extraction of Li takes place from both the transition metal layer and Li layers, as shown by the changes in the two characteristic peaks at 445 and 544 cm^{-1} [66]. After the removal of oxygen, the transition metal ions diffuse to the vacant sites.

7 Nanostructured materials for advanced Li-ion battery electrodes

The interest in using nanomaterials for advanced Li-ion battery electrodes stems from their high storage capacity and cycle life. The most important material, considered suitable to replace graphite anodes, proved to be nanostructured silicon (Si) such as Si nanotubes used for battery anodes [67], Si nanowires [68–70] and Si nanoparticles inserted in graphene sheets [71] Nanocomposites including Si nanoparticles have also been used as anode materials [72]. Mesoporous carbon particles filled with tin, tin sulfide, and vanadium oxide nanoparticles have been prepared

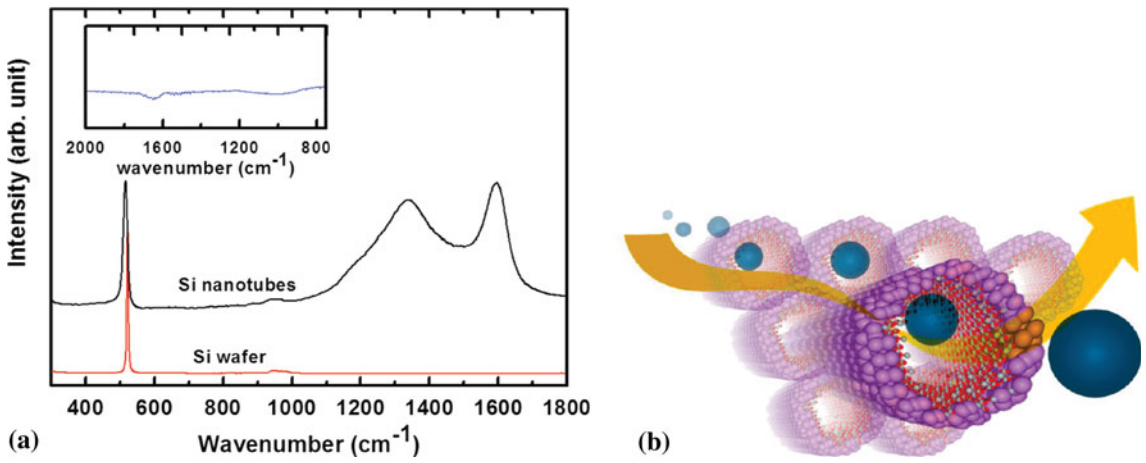

Fig. 22 **a** Raman spectra of Si nanotubes and Si wafer reference. The *inset* is the FTIR spectrum of Si nanotubes. **b** Schematic diagram of Li-ion pathway in the Si nanotube. Reprinted from [67]. Copyright (2009), with the permission of American Chemical Society

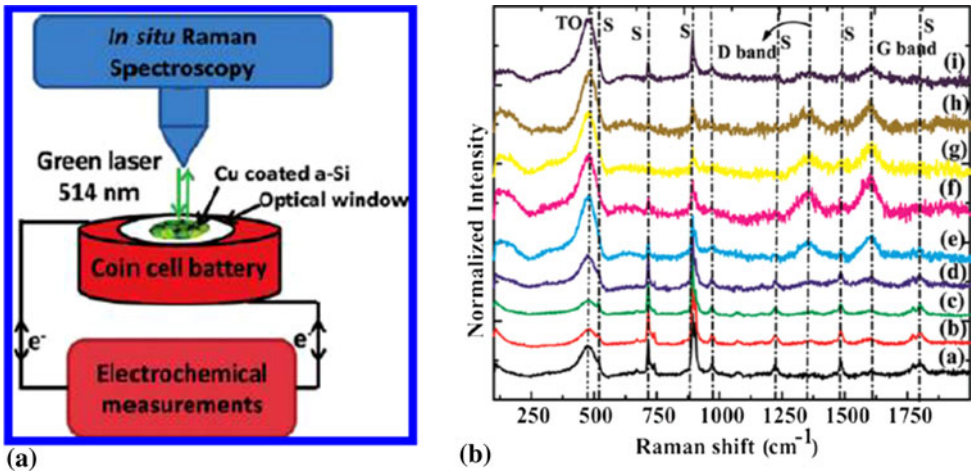

Fig. 23 **a** Illustration of the in situ Raman measurements in a coin cell battery. **b** In situ Raman measurements of a-Si:H particles with the electrode composition of 70:20:10 of active a-Si:H, conductive carbon Super-P, and binder PVDF. TO is the phonon mode of a-Si:H, and S represents the solvent peaks. D- and G-bands correspond to the conductive carbon present in the electrode. The Raman signatures were measured at different potentials during the charging and discharging process corresponding to (*a*) initial, (*b*) 2 V, (*c*) 1.2 V, (*d*) 0.65 V, (*e*) 0.57 V, (*f*) 0.35 V, (*g*) 0.1 V, (*h*) 2nd cycle lithiation 0.19 V, and (*i*) 2nd cycle de-lithiation 0.58 V. Reprinted from [76]. Copyright (2010), with permission from the American Chemical Society

and tested. A short review on the new nanomaterials used in Li batteries can be found in Aurbach [73]. In addition to nanostructured Si, -MnO2 nanoparticles were used for the fabrication of transparent Li-ion batteries [74]. In most of these studies, Raman spectra were used in order to clarify the structural changes upon lithiation. (see also reference [75]) For example, the Raman spectra of Si nanotubes and a wafer reference are shown in Fig. 22.

The authors assigned the sharp band in the Raman spectrum at around 516 cm^{-1} to the Si–Si stretching mode (same as in the wafer), and the weak peak around 957 cm^{-1} to the amorphous Si–Si stretching mode (same in the wafer). The strong peaks at 1,360 and 1,580 cm^{-1} are assigned to the D-band, related to the disorder in the material and the G-band (graphene band) of carbon, respectively. In this work, the Si nanotubes are coated with carbon which promotes the SEI formation. The Raman spectra have confirmed the presence of a very thin coating of carbon. The very high reversible charge capacity (3,247 mA/h/g) of the nanotubes is accounted for by the increased accessible area of the electrolyte, and the Li ions being able to intercalate both in the interior and the exterior of the nanotubes as shown in Fig. 22b.

Using nanostructures such as nanowires, nanotubes, nanorods, etc., is one of the approaches to overcome the problem of volume expansion and contraction of Si upon

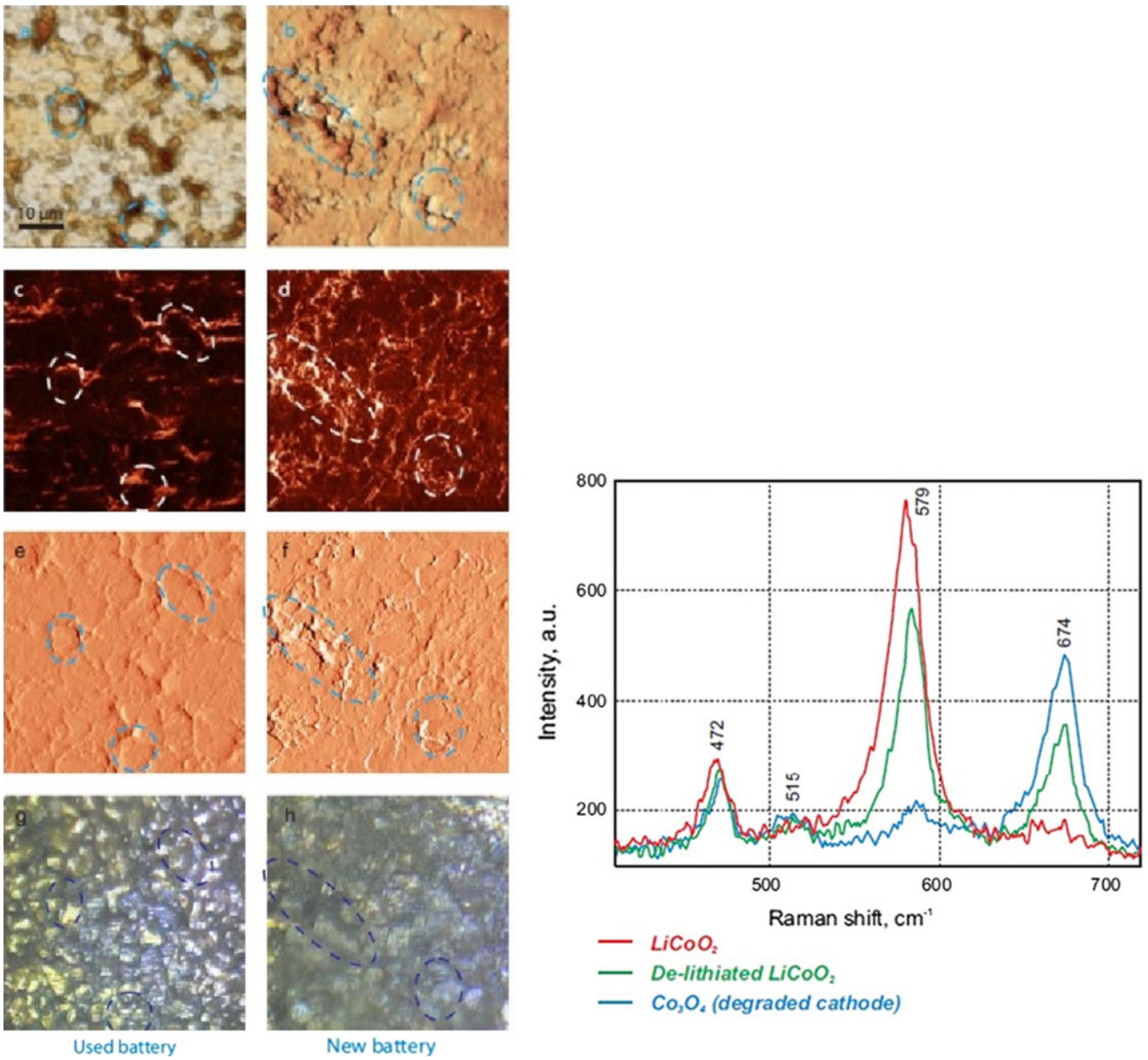

Fig. 24 **a**, **c** Exhibit high roughness and grain structure, typical for used batteries. **b** Raman spectra of cathode: $LiCoO_2$ (*red*), de-lithiated $LiCoO_2$ (*green*), and Co_3O_4 (*blue*). The resolved bands may be related with the structural distortion or the surface change during the extraction of Li. Reprinted from [86]

lithiation/delithiation [77]. The approach used in Murugesan's work is coating Si with copper (Fig. 23).

The in situ Raman measurements of a-Si:H particles have shown important changes in Raman scattering intensity at 1,600 cm^{-1} (G-band of graphitic carbon) because of the lattice relaxation of carbon due to Li insertion. Raman spectra proved that Li is intercalated into the carbon component of the electrode and provided mechanistic insight into the lithiation/de-lithiation process and the role of the Cu layer. The authors suggested that the principal role of the copper coating is to suppress the decomposition of the solvent. The advantages and disadvantages of nanomaterials in Li batteries, supercapacitors, and fuel cells are discussed in an excellent review article by Arico et al. [78].

The role of nanomaterials in terms of electrochemical performance is discussed in Lee and Cho's review [79] as well as in the paper of Liu et al. [80]. The excellent rate performance of nanostructured materials is accounted for by the short diffusion length.

Nanostructured transitional metal oxides were successfully investigated for both electrochromic and Li-ion battery technologies [81]. Crystalline tungsten oxide nanorods

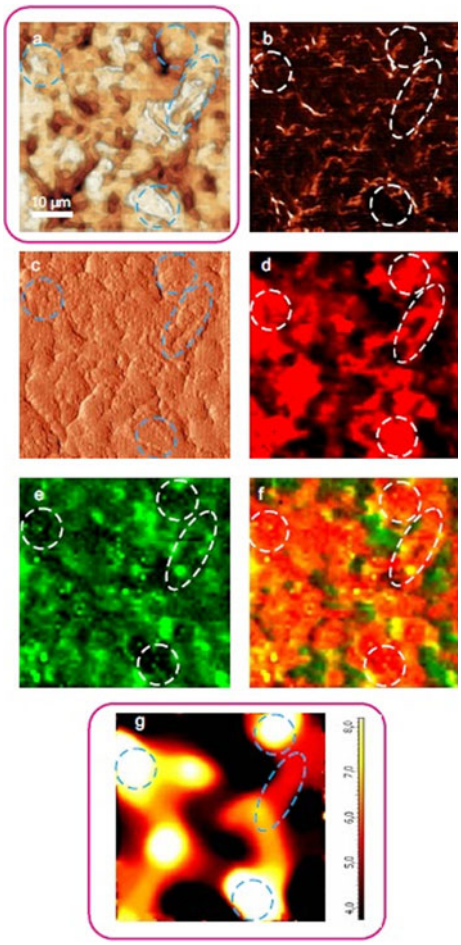

Fig. 25 AFM and Raman images from the same place of the new cathode: **a** AFM topography height, **b** phase, **c** magnitude; **d** Raman intensity map corresponding to the 579 cm^{-1} peak, **e** Raman intensity map using 674 cm^{-1} peak, **f** chemical map (*red color* corresponds to the $LiCoO_2$, *green color* is de-lithiated $LiCoO_2$ (Co_3O_4 is absent on this cathode, because the intensity of peak at 674 cm^{-1} is never ranked over the intensity of peak 579 cm^{-1}); **g** ratio of peak intensities at 579 and 674 cm^{-1}. *Black color* corresponds to the de-lithiated cathode; *yellow color* corresponds to the intercalated one. Reprinted from [86]

and nanoparticles as well as molybdenum oxide nanostructures were incorporated into porous films and used for electrochromic applications with very good results. Spherical molybdenum oxide nanoparticles were tested for battery applications and a high reversible capacity was found. Raman spectra in this work were used mostly to assess the degree of crystallinity. This publication is important because for the first time, the authors emphasized the similarity between electrochromic materials and anode materials for Li-ion batteries. Nanostructured tungsten oxide for electrochromic applications was also prepared by Badilescu et al. [82, 83] and Li [84] where Raman analysis revealed the correlation between the presence of the ε-monoclinic crystal phase of the tungsten oxide and the electrochromic performance.

8 Combined AFM and Raman microscopy for advanced analysis of batteries

8.1 Introduction to the combined instrumentation (AFM–Raman)

Raman spectrometers can be easily incorporated into non-optical microscopes, for example, SEM and AFM. Integrated systems enable users to perform two or more analytical techniques on the same sample region, under the same conditions, in a single instrument [85].

The combined technique correlates the chemical information, obtained through the Raman spectra, with image-based information. Manufacturers now propose two types of combined instruments—integrated and interfaced systems, respectively. Fully integrated systems are offered by manufacturers such as NTegra Spectra, WiTech, Horiba, and others. The manufacturers had to solve many problems related to the inherent differences between the two methods, for example, in acquisition times and spatial resolution.

8.2 AFM–Raman study of a Li battery

Cathodes from used batteries were analyzed by using combined AFM and Raman microscopy [86, 87].

The method allows finding the distribution of degraded areas on the surface of the positive electrode ($LiCoO_2$). The simultaneous recording of AFM and Raman images is done on an NTEGRA Spectra (NT-MDT) instrument, integrated with Renishaw inVia Raman spectrometer. The "old" laptop battery, after 1,200 charging–frecharging cycles, had only 25 % of its nominal capacity while the second was new, charged to ~65 %. The AFM results provided information about the size, shape, and orientation of the particles. The results showed that the cathode from the new battery is much smoother than the one of the used one. In the aged battery, the extraction of Li has caused the crystal cell to expand and individual microcrystals are seen on the surface. Both the state of the surface and the corresponding spectra depend on the electrochemical history. AFM images from both batteries are shown in Fig. 24.

The two strong bands observed at 472 and 579 cm^{-1} correspond to υ_2 (E_g), O–Co–O bending and υ_1 (A_{1g}), Co–O stretching modes, respectively. During the charging (extraction of Li), the main peaks undergo a small shift and the intensity of the 515 and 674 cm^{-1} band increases. The two bands are assigned to the vibrational modes of Li_2O and Co_3O_4, the degradation products of the cathode. The figure shows 2D Raman and AFM maps from the same place of the cathode removed from the new battery (Fig. 25).

By studying simultaneously the AFM and the Raman images, important information on the electrode material

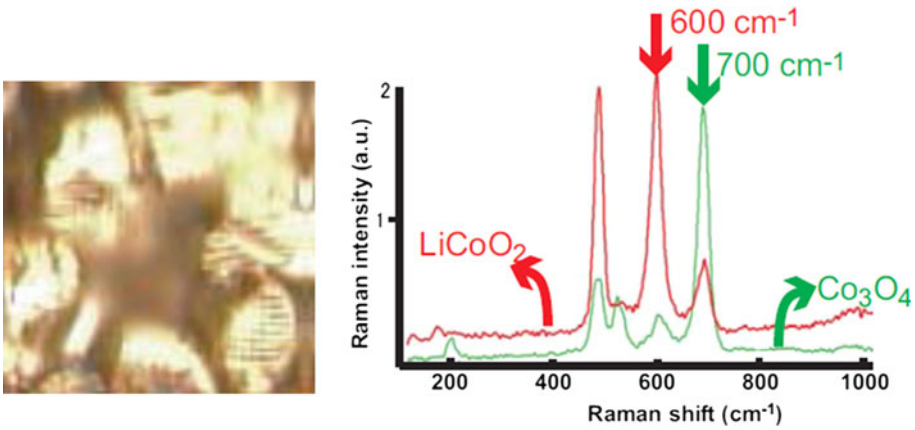

Fig. 26 Surface observation of the positive electrode of a Li-ion battery by optical microscope. Raman spectra of $LiCoO_2$ and Co_3O_4 on Li-ion battery positive electrode surface. Reprinted from [87]

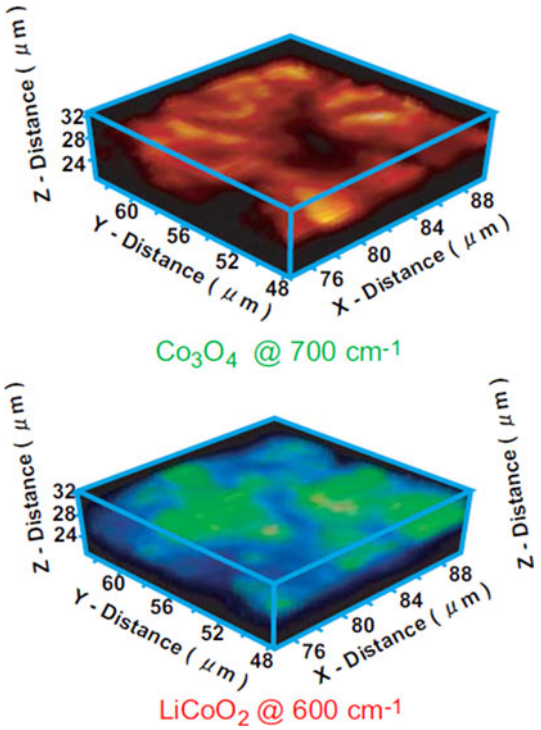

Fig. 27 3D Raman images of positive electrode in a Li-ion battery. Reprinted from [87]

can be found. For example, because the main degradation product of the positive electrode ($LiCoO_2$) is Co_3O_4, by using their specific bands, 3D images show the state of the degradation of the electrode (Figs. 26, 27).

An intriguing use of the ability of Raman spectroscopy to evaluate the composition changes at the grain boundary of a particle in an electrode is proposed by Jebaraj and Scherson in a recent paper. This work shows the continuing trend for miniaturization in spectroelectrochemistry, the implementation of new methods capable to investigate microparticle electrodes and single-particle microbatteries [88]. These changes can be correlated with the state of charge of the particles. For this purpose, the authors built a measurement cell capable to perform micro-Raman spectroscopy on a single particle and correlate it with voltammetric data measured on that particle. They studied graphite microflakes, particles of $LiMn_2O_4$, as well as single-particle microbatteries belonging to other chemistries [Zn | MnO_2 and $Ni(OH)_2$ | MH]. Based on the success of this approach, the authors are looking at the use of Raman microscopy for the examination of the edge surface of an operating battery during charging and discharging. Such information is highly relevant for the validation of the macroscale theoretical models of battery behavior.

9 Other in situ techniques

Li-ion batteries are complex electrochemical systems and their investigation requires fairly sophisticated methods.

Different characterization techniques have been used for the study of battery materials, either alone or in tandem with Raman spectroscopy. The intent in this section is to mention their existence, and the type of information they provide, as opposed to giving a comprehensive description of all the in situ techniques. This information, as provided by state-of-the-art, noninvasive techniques, is briefly described below.

For example, while X-ray diffraction was used almost from the beginning of battery science to measure the lattice changes of the Li^+ insertion host [24] during the last decade, new methods based on X-rays joined the arsenal and enriched the information. Among them are methods such as X-ray absorption spectroscopy, X-ray absorption near-edge structure (XANES), and extended X-ray absorption fine structure (EXAFS) as well as XPS also called electron spectroscopy for chemical analysis (ESCA) [89].

All these methods are element specific, sensitive, and require only small sample volumes. The most recent techniques (XANES and EXAFS) are able to indicate any

change in the oxidation states of elements such as Ni, Co, and Mn. XPS and ESCA allow the analysis of all the elements in the outermost 10 nm of the surface as well as the chemical composition of SEI on a graphite anode [90]. However, because of the high-energy photons, there is always a risk of radiation damage [13, 15]. The evolution of in situ X-ray diffraction techniques and their benefits to the field of energy storage is described in the comprehensive review paper of Morcrette et al. [91].

In situ neutron diffraction has proved to be even more sensitive to Li than XRD [92]. Light elements such as Li, H, and O can only be localized by using neutrons. At the same time, by using this method, neighboring elements can be distinguished easily, while by XRD this is not possible. However, because of the weak interaction of neutrons with matter, measurements need a considerable amount of material and/or long acquisition times. In order to better define the diffraction volume, circular neutron diffraction cells have been designed [93]. Lattice parameters as well as the phases present in the electrodes in their charged states can be determined. For example, $LiCoO_2$ has been found as a layered and a cubic spinel-type phase and both of them insert Li^+.

Neutrons have a high penetrating power, which means that the measurements do not represent only the surface region of the sample. Both electrodes can be observed simultaneously, and spatially resolved measurements can be conducted by defining a scattering volume and thus the areas where their degradation begins can be identified [94]. By using this technique, the authors demonstrated that the degradation (capacity loss) is spatially heterogeneous in both the graphite anode and the spinel-based cathode of commercial Li-ion batteries [95].

The NMR techniques provide chemical information based on chemical shift of various nuclei [96, 97]. Solid-state ^{7}Li NMR proved to be useful for the study of the evolution of SEI on graphite anodes when different alkyl carbonates were used as electrolytes [98].

Ex situ NMR studies may give interesting information on electrode materials because they allow the use of modern methods such as magic angle spinning. In these studies, the battery, after being cycled to a specific state of charge, is taken apart to perform NMR. However, *ex situ* methods fail to give information on short-lived species. In situ NMR studies make use of ^{7}Li-quadrupole nucleus with a spin $I = 3/2$, more sensitive than ^{6}Li. The first ^{7}LiNMR studies were carried out on graphitic carbon. Distinct Li NMR peaks were evidenced for each stage with the peaks shifted to high frequencies with increasing Li content. In situ NMR was found to be a quantitative and nondestructive method to study the conditions under which dendrites form, but lacks spatial information. However, the noninvasive visualization of Li microstructures on the negative electrode became possible only after the development of the ^{7}Li MRI technique, and overcoming the technical difficulties related to the orientation of electrodes to the RF field [99]. It was found that the rate of dendrite formation is different under different electrochemical conditions. Moreover, with this technique, dendritic structures can be distinguished from moss and quantified. The capability of visualizing the irregular porous microstructures has been shown to be very important for understanding how to prevent battery overheating and/or short-circuiting that may result in ignition.

Raman spectroscopy was often used in tandem with in situ FTIR, either in external or in internal reflectance mode, because of the strong absorption of the electrolyte solution. However, the interpretation of spectra, especially those of SEI, is sometimes difficult, because of the overlapping weak bands. The experimental approach and infrared data on battery materials can be found in some excellent review papers [38, 100]. In situ AFM and SEM have been used since a long time to quantify the expansion of the grapheme planes during the intercalation of Li^+ [16, 101, 102]. AFM–Raman integrated systems have been discussed in Sect. 8.

All these methods extract and interpret information on the electrode materials and the electrode/electrolyte interphase to probe the evolution of the electrochemical behavior under various conditions. As discussed in Sect. 7, the most efficient way to investigate battery materials is to correlate the chemical information, obtained through Raman, IR, and NMR spectra, with image-based information provided by the most sophisticated microscope systems.

One of the most relevant areas of activity in battery science, for which the availability of the real-time information regarding the evolution of structure and chemical composition during battery charging and discharging is essential, is battery modeling [103]. The precise understanding of the dynamic nature of SEI, of the interfacial reactions, and of the nature of the different processes leading to changes in the internal resistance requires a significant input based on data provided by the techniques described here. The synergism between the experiment and modeling is one of the most powerful tools at our disposal for progress in battery science and technology. Raman-based investigation techniques play an essential role in this ongoing effort.

10 Conclusion

In this review we have demonstrated that the Raman techniques, in tandem with other methods, were extremely helpful in understanding the mechanisms of Li intercalation and were instrumental in screening new electrode

materials for LIB. In situ Raman studies of battery components closely followed the recent advances in the development of Raman technology. Chronologically, this trend started with Raman studies on HOPG and on other types of carbon, a logical beginning, taking into account the already existing substantial knowledge on graphite and the corresponding stage structure of GICs. By studying the mechanism of insertion of Li into different types of carbon used as anode materials, through simultaneous Raman and electrochemical measurements, it was possible to connect the capacity of intercalation to the degree of disorder of the material. Further studies, made possible by the implementation of confocal Raman microscopy, focused on the polymer electrolyte and its concentration gradient and later on the characterization of oxide materials in positive electrodes of Li-ion cells. After the Raman arsenal was enriched by the discovery of SERS, the application of this new technique to the battery science, contributed to understanding the electrode/electrolyte phenomena.

As we have emphasized, the most important advancement during the almost 20 years of Raman work discussed in this review was the discovery and development of confocal Raman microscopy. By using this technique, the simultaneous investigation of electrodes and electrolyte became possible, together with quantitative data such as the concentration gradient of the electrolytes, the composition of SEI, etc. Most importantly, the confocal microscopy in integrated systems allowed the study of the degradation of electrode materials under different conditions and helped to solve safety issues.

In conclusion, the analysis of data obtained either only by Raman spectroscopy or through a combined methodology, by using more and more sophisticated electrochemical cells, points toward an unprecedented expansion of the spectroelectrochemical methods in the field of Li-ion batteries.

References

1. Yet-Ming C (2010) Science 330:1485
2. Raman CV, Krishnan KS (1928) Nature 121:711
3. Landsberg G, Mandelstam L (1928) Naturwissenschaften 16:557
4. Delhaye M, Migeon M (1966) C R Acad Sci Paris 262:702
5. Delhaye M, Dhamelincourt P (1975) J Raman Spectrosc 3:33
6. Delhaye M, Dhamelincourt PP, Wallart F, Lechlerg M, N'Guyen AT, London DO (1979) Anal Chem 51:414A
7. Andersen ME, Muggli RZ (1981) Anal Chem 53:1772
8. Adar F, Delhaye M, DaSilva E (2007) J Chem Educ 84:50
9. Matousek P, Clark IP, Draper ERC, Morris MD, Goodship AE, Everall N, Towrie M, Finney WF, Parker AW (2005) Appl Spectrosc 59:393
10. DeGraff BA, Hennip M, Jones JM, Salter C, Schaertel SA (2002) Chem Educ 7:15
11. Baddour-Hadjean R, Pereira-Ramos J-P (2010) Chem Rev 110:1278
12. Amaraj SF, Aurbach D (2011) J Solid State Electrochem 15:877
13. Aurbach D, Zaban A, Gofer Y, Ein Ely Y, Weissman I, Chusid O, Abranson O (1995) J Power Sources 54:76
14. Odziemkowski M, Irish DE (1992) J Electrochem Soc 139:3063
15. Verma P, Maire P, Novák P (2010) Electrochim Acta 55:6332
16. Campana FP, Kötz R, Vetter J, Novák P, Siegenthaler H (2005) Electrochem Commun 7:107
17. Dolle M, Grugeon S, Beaudoin B, Dupont L, Tarascon J-M (2001) J Power Sources 97–98:104
18. Inaba M, Yoshida H, Ogumi Z, Abe T, Mizutani Y, Asano M (1995) J Electrochem Soc 142:20
19. Inaba M, Yoshida H, Ogumi Z (1996) J Electrochem Soc 143:2572
20. Zanini M, Basu S, Fischer JE (1978) Carbon 16:211
21. Eklund PC, Dresselhaus G, Dresselhaus MS, Fischer JE (1980) Phys Rev 21B:4705
22. Doll GL, Eklund PC (1987) Phys Rev 36B:4940
23. Underhill C, Leung SY, Dresselhaus G, Dresselhaus MS (1979) Solid State Commun 29:700
24. Dahn JR (1991) Phys Rev B44:9170
25. Endo M, Kim C, Karaki T, Fujino T, Matthews MJ, Brown SDM, Dresselhaus MS (1998) Synth Met 98:17
26. Occupational Safety & Health Administration, OSHA Technical Manual (OTM), Section III, Chap 6, Laser Hazards, United States, Department of Labor (1999)
27. Endo M, Kim C, Nishimura K, Fujino T, Miyashita K (2000) Carbon 38:183
28. Rey I, Bruneel J-L, Grondin J, Servant L, Lassegues JC (1998) J Electrochem Soc 145:3034
29. Rey I, Lassègues JC, Baudry P, Majastre H (1998) Electrochim Acta 43:1539
30. Minsky M (1988) Scanning 10:128
31. Dhamelincourt P, Barbillat J, Delhaye M (1993) Spectrosc Eur 5:16
32. http://www.olympusconfocal.com. Accessed 15 Nov 2012
33. Princeton Instruments www.placton.com. Accessed 15 Nov 2012
34. Rey I (1997) Thesis, Université de Bordeaux
35. Doyle M, Fuller TF, Newman J (1993) J Electrochem Soc 140:1526
36. Brissot C, Rosso M, Chazalviel J-N, Lascaud S (1999) J Electrochem Soc 146:4393
37. Brissot C, Rosso M, Rosso JN, Chazalviel JN, Lascaud S (2001) J Power Sources 94:212
38. Novák P, Panitz J-C, Joho F, Lanz M, Imhof R, Coluccia M (2000) J Power Sources 90:52
39. Panitz J-C, Joho F, Novak P (1999) Appl Spectrosc 53:1188
40. Aurbach D, Markovski B, Lavi MD, Levi E, Schechter A, Moshkovich M, Cohen Y (1999) J Power Sources 81/82:95
41. Novák P, Joho F, Lanz M, Rycart B, Panitz J-C, Alliata D, Kötz R, Haas O (2001) J Power Sources 97–98:39
42. Zane D, Antonini A, Pasquali M (2001) J Power Sources 97–98:146
43. Aurbach D, Markovsky B, Weissman I, Levi E, Ein-Eli Y (1999) Electrochim Acta 45:67
44. Novák P, Goers D, Hardwick L, Holzapfel M, Scheifele W, Ufheil J, Würsig A (2005) J Power Sources 146(2005):15–20
45. Besenhard JO, Winter M, Yang J, Biberacher W (1995) J Power Sources 54:228
46. Xu K (2010) Energies 3:135
47. Martha SK, Markevich E, Burgel V, Salitra G, Zinigrad E, Markovsky B, Sclar H, Pramovich Z, Heik O, Aurbach D, Exnar I, Buqa H, Drezen T, Semrau G, Schmidt M, Kovacheva D, Saliyski N (2009) J Power Sources 189:288

48. Fleischmann M, Hendra PJ, MacQuillan A (1974) Chem Phys Lett 26:163
49. Kneipp K, Kneipp H, Itzkan I, Dasari RR, Feld MS (1999) Chem Rev 99:2957
50. Moskovits M (1985) Rev Mod Phys 57:783
51. Otto A, Mrozek I, Grabborn H, Akemann W (1992) J Phys Condens Matter 4:1143
52. Furtak TE (1982) J Electroanal Interfacial Electrochem 150:375
53. Badilescu S, Ashrit PV, Vo-Van T, Badilescu II (1989) Appl Spectrosc 43:549
54. Irish DE, Deng Z, Odziemkowski M (1995) J Power Sources 54:28
55. Li G, Li H, Mo Y, Huang X, Chen L (2000) Chem Phys Lett 330:249
56. Li G, Li H, Mo Y, Chen L, Huang X (2002) J Power Sources 104:190
57. Naudin C, Bruneel JL, Chami M, Desbat B, Grondin J, Lassègues JC (2003) J Power Sources 124:518
58. Luo Y, Wen-Bin C, Xue-Kun X, Scherson DA (2004) Electrochem Solid-State Lett 2004:E1
59. Novak P, Goers D, Hardwick L, Holzapfel M, Scheifele W, Ufheil J, Würsig A (2005) J Power Sources 146:15
60. Hardwick LJ, Hahn M, Ruch P, Holzapfel M, Scheifele W, Buqa H, Krumeich F, Novák P, Kötz R (2006) Electrochim Acta 52:675
61. Ruch PW, Hardwick LJ, Hahn M, Foelske A, Kötz R, Wokaun A (2009) Carbon 47:38
62. Markevich E, Baranchugov V, Salitra G, Aurbach D, Schmidt MA (2008) J Electrochem Soc 155:A132
63. Haijun Yu and Haoshen Zhou (2013) J Phys Chem Lett 4:1268–1280
64. Francis Amalraj S, Markovsky B, Sharon D, Talianker M, Zinigrad E, Persky R, Haik O, Grinblat J, Lampert J, Schultz-Dobrick M, Garsuch A, Burlaka L, Aurbach D (2012) Electrochim Acta 78:32–39
65. Lanz P, Villevieille C, Novák P (2013) Electrochim Acta 109:426–432
66. Singh G, West WC, Soler J, Katiyar RS (2012) J Power Sources 218:34–38
67. Park M-H, Kim MG, Joo J, Kim K, Kim J, Ahn S, Cui Y, Cho J (2009) Nano Lett 9:3844
68. Chan CK, Hailin P, Gao L, McIlwrath K, Xiao Feng Z, Huggins RA, Cui Y (2008) Nat Nanotechnol 3:31
69. Li-Feng C, Ruffo R, Chan CK, Hailin P, Yi C (2009) Nano Lett 9:491
70. Chan CK, Patel RN, O'Connell MJ, Korgel BA, Cui Y (2009) ACS Nano 4:1443
71. Zhou X, Yin Y-X, Wan L-J, Guo Y-G (2012) Chem Commun 48:2198
72. Chen M, Du C, Wang L, Yin G, Shi P (2012) Int J Electrochem Sci 7:819
73. Aurbach D (2005) J Power Sources 146:71
74. Yang Y, Jeong S, Hu L, Wu H, Wuo Lee S, Cui Y (2011) PNAS 108:13013
75. Stura E, Nicolini C (2006) Anal Chim Acta 568:57
76. Song T, Xia JL, Lee JH, Lee DH, Kwon MS, Choi J (2010) Nano Lett 10:1710
77. Murugesan S, Harris JT, Korgel BA, Stevenson KJ (2012) Chem Mater 24:1306
78. Aricò AS, Bruce P, Scrosati B, Tarascon J-M, Van Schalkwijk W (2005) Nat Mater 4:366
79. Lee KT, Cho J (2011) Nano Today 6:28
80. Liu HK, Wang GX, Guo ZP, Wang JZ, Konstantinov V (2007) J New Mater Electrochem Syst 10:1014
81. Dillon AC, Mahan AH, Deshpande R, Parilla PA, Jones KM, Lee S-H (2008) Thin Solid Films 516:794
82. Badilescu S, Ashrit PV (2003) Solid State Ion 158:187
83. Badilescu S, Minh-Ha N, Bader G, Ashrit PV, Girouard FE, Vo-Van T (1993) J Mol Struct 297:393
84. Li CP, Wolden CA, Dillon AC, Tenent RC (2012) Sol Energy Mater Sol Cells 99:50
85. B. Foster (2007) Amer Lab, 39:March
86. http://www.azonano.com/article.aspx?ArticleID=3053. Accessed 10 May 2013
87. (http://www.tokyoinst.co.jp). Accessed 15 May 2013
88. Jebin A, Jebaraj J, Scherson DA (2013) Acc Chem Res 46:1192
89. Shearing P, Wu Y, Harris SJ, Brandon N (2011) Electrochem Soc Interface 20:43
90. Lee JT, Nitta N, Benson J, Magasinski A, Fuller TF, Yushin G (2013) Carbon 52:388
91. Morcrette M, Chabre Y, Vaughan G, Amatucci G, Leriche J-B, Patoux S, Masquelier C, Tarascon J-M (2002) Electrochim Acta 47:3137
92. Sharma N, Peterson VK, Elcombe MM, Avdeev M, Studer AJ, Blagojevic N, Yussoff R, Kamarulzaman N (2010) J Power Sources 195:8258
93. Godbole VA, Heß M, Villevieille C, Kaiser H, Colin J-F, Novak P (2013) RSC Adv 3:757
94. Xun-Li W, Ke A, Lu C, Zhili F, Nagler SE, Daniel C, Rhodes KJ, Stoica D, Skorpenske HD, Chengdu L, Wei Z, Joon K, Yue Q, Stephen J, Harris SJ (2012) Sci Rep 2:747
95. Lu C, Ke A, Zhili F, Chengdu L, Harris SJ (2013) J Power Sources 236:163
96. Trease NM, Köster TKJ, Grey CP (2011) The Electrochemical Society Interface Fall:69
97. Dupré N, Cuisinier M, Guyomard D (2011) The Electrochemcial Soc Interface Fall:61
98. Smart MC, Ratnakumar BV, Surampudi S, Wang Y, Zhang X, Greenbaum SG, Hightower A, Ahn CC, Fultz B (1999) J Electrochem Soc 146:3963
99. Chandrashekar S, Trease NM, Hee Jung C, Lin Shu D, Grey CP (2012) Nat Mater 11:311
100. Aurbach D (2000) J Power Sources 89:206
101. Aurbach D, Cohen Y (1996) J Electrochem Soc 143:3525
102. Kong F, Kostecki R, Nadeau G, Song X, Zaghib K, Kinoshita K, McLarnon F (2001) J Power Sources 97–98:58
103. Yang Y, Jeong S, Hu L, Wu H, Wou Lee S, Cui Y (2011) PNS 108:13013